Journal of Engineering Mathematics **39:** 87–130, 2001.

Asymptotic analysis of the steady-state and time-dependent Berman problem

J. R. KING and S. M. COX
School of Mathematical Sciences, University of Nottingham, University Park, Nottingham NG7 2RD, UK (e-mail: john.king@nottingham.ac.uk; stephen.cox@nottingham.ac.uk)

Received 14 December 1999; accepted in revised form 14 September 2000

Abstract. The Berman problem for two-dimensional flow of a viscous fluid through an infinite channel is studied. Fluid motion is driven by uniform suction (or injection) of fluid through the upper channel wall, and is characterised by a Reynolds number R; the lower wall is impermeable. A similarity solution in which the streamfunction takes the form $\psi = -x\mathcal{F}(y,t)$ is examined, where x and y are coordinates parallel to and normal to the channel walls, respectively. The function $\mathcal{F}$ satisfies the Riabouchinsky–Proudman–Johnson equation, a partial differential equation in y and t; steady flows satisfy an ordinary differential equation in y. The steady states are computed numerically and the asymptotics of these solutions described in the limits of small wall suction or injection, large wall injection and large wall suction, the last of these being given more concisely and more accurately than in previous treatments. In the time-dependent problem, the solution appears to be attracted to a limit cycle when $R \gg 1$ (large wall suction). This solution has been computed numerically for $\epsilon = 1/R$ down to 0·011, but the structure of the solution makes further numerical progress currently infeasible. The limit cycle consists of several phases, some with slow and others with very rapid evolution. During one of the rapid phases, the solution achieves a large amplitude, and this feature of the solution lies behind the practical difficulties encountered in numerical simulations. The profile of the solution is plotted during the various phases and corresponding asymptotic descriptions are given. An exact solution to the Riabouchinsky–Proudman–Johnson equation covers most of the phases, although separate discussion is required of the boundary layers near the two walls and an interior layer near a zero of $\mathcal{F}$. Particular consideration is required when this zero approaches the upper channel wall.

Key words: similarity solution, Navier–Stokes equations, Berman problem, asymptotics, channel flow.

1. Introduction

We consider a similarity solution of the Navier–Stokes equations for plane flow of a viscous fluid confined between parallel walls. The flow is driven by uniform withdrawal (or injection) of the fluid through the upper channel wall, the lower wall being impermeable. The problem is characterised by a Reynolds number R, based on the speed at which fluid is withdrawn from the channel, and our particular interest is in the asymptotic structure of the flow when this Reynolds number is large.

The governing Navier–Stokes equations and boundary conditions permit a flow whose streamfunction ψ takes the form $-x\mathcal{F}(y,t)$, where x is the coordinate parallel to the channel walls, y is the normal coordinate and t is time. The governing partial differential equation for the similarity function $\mathcal{F}$ is due to Riabouchinsky [1] – see also Proudman and Johnson [2]; as a special case, steady flows (those for which $\mathcal{F} = f(y)$) satisfy an ordinary differential equation [3] studied by Berman [4] in the context of channel flow. We shall refer to the problem of determining $\mathcal{F}(y,t)$ for various Reynolds numbers as the Berman problem.

The large Reynolds number asymptotic behaviour of the steady solutions has proved remarkably subtle, and was one of the first applications of exponential asymptotics in fluid mechanics (by Terrill [5]; see also [6] and [7]). It is this large Reynolds number behaviour, of both steady and unsteady solutions, that we primarily treat below.

The Berman problem was originally investigated in the case where both channel walls are equally permeable (see, for example, [4, 8, 9]). The extension to a more general case, where the fluid is withdrawn from the two channel walls at different rates, has also been carried out [10–15].

The limiting case of 'complete' asymmetry, with one permeable and one impermeable wall, has previously been investigated [7, 15, 16], and it is this problem that is addressed in this paper. In this case, there is a unique steady solution for all values of R, except in the range $7{\cdot}05 \approx R_1 < R < R_2 \approx 7{\cdot}31$, where there are three solutions [15, 16]. After formulating the problem in Section 2, in Section 3 we compute the steady solutions numerically and offer asymptotic solutions in the three limits of large wall injection, large wall suction, and small wall suction or injection. Numerical solution of the ordinary differential two-point boundary-value problem is simplified by means of a rescaling due to Terrill [8] which converts it into an initial-value problem. This rescaling allows calculation of numerical solutions at much larger Reynolds numbers than would otherwise be possible by direct calculation, for example by shooting from the channel walls and matching.

It is possible to compute the stability of the steady flows to disturbances which are also of the similarity form $\psi = -x\mathcal{F}(y,t)$. It is then found [15] that the steady state becomes unstable in a Hopf bifurcation at $R = R_3$, where $R_3 \approx 12{\cdot}755$. Numerical evidence suggests that this bifurcation is supercritical, and that a limit cycle exists for $R > R_3$. This limit cycle seems to be stable (within the context of the Riabouchinsky–Proudman–Johnson equation, henceforth the RPJ equation) for all values of the Reynolds number at which we have carried out numerical simulations of the initial-value problem (see Section 4). As the Reynolds number is increased, the limit cycle separates into slow and fast phases of evolution. During one of the fast phases, the solution gains large amplitude, and this combination of rapid evolution and large amplitude makes reliable numerical simulation difficult. Indeed with our (admittedly rather unsophisticated) numerical scheme we have been unable to compute the limit cycle reliably beyond $R \approx 100$ without the run times becoming prohibitively long. The asymptotic structure of the limit cycle, described in Sections 5, 6 and 7, makes clear why such numerical difficulties are encountered. We note that there have heretofore been very few asymptotic treatments of time-dependent solutions to the RPJ equation, a notable exception being the blow-up study of Grundy and McLaughlin [17].

We discuss our results in Section 8, and make our concluding remarks in Section 9. Appendix A outlines the general solution to the inviscid RPJ equation in the case of zero pressure and also analyses its similarity solutions, these playing a crucial role in Sections 6 and 7. Appendix B discusses symmetry (and related) properties of the full (viscous) RPJ equation. We note that the notation of Section 3 sometimes departs from that of the remainder of the paper.

2. The Berman problem

We consider two-dimensional flow of a Newtonian fluid with kinematic viscosity ν in a channel of half-width h. The flow is driven by uniform withdrawal of the fluid through the upper

channel wall with speed V; the lower channel wall is impermeable. After adopting the scales h and h/V for length and time, respectively, we note that a particular class of solutions to the governing (dimensionless) Navier–Stokes equations may be written in terms of a stream-function $\psi(x, y, t)$ via $\psi = -x\mathcal{F}(y, t)$, where x and y are coordinates parallel and normal to the channel walls, respectively. The velocity field is then given by $u = \partial\psi/\partial y = -x\mathcal{F}_y$, $v = -\partial\psi/\partial x = \mathcal{F}$. After elimination of the pressure from the Navier–Stokes equations, we find, for the similarity flow of interest, that the function $\mathcal{F}$ satisfies the RPJ equation [9]

$$\mathcal{F}_{yyt} = \epsilon\mathcal{F}_{yyyy} + \mathcal{F}_y\mathcal{F}_{yy} - \mathcal{F}\mathcal{F}_{yyy}, \tag{1}$$

where $R = hV/\nu$ is the Reynolds number and $\epsilon = R^{-1}$, subject to the boundary conditions

$$\mathcal{F}(-1, t) = \mathcal{F}_y(-1, t) = \mathcal{F}_y(1, t) = 0, \qquad \mathcal{F}(1, t) = 1, \tag{2}$$

corresponding to normal suction (for $\epsilon > 0$) or injection (for $\epsilon < 0$) through the upper wall at $y = 1$, and an impermeable no-slip lower wall at $y = -1$. For numerical simulation of (1) it is useful to note that this equation may be integrated once in y to give [1, 2]

$$\mathcal{F}_{yt} = \epsilon\mathcal{F}_{yyy} + \mathcal{F}_y^2 - \mathcal{F}\mathcal{F}_{yy} + p(t), \tag{3}$$

where $p(t)$ is a function of integration, with the fluid pressure being $\hat{p}(y, t)+x^2 p(t)/2$, where $\hat{p}$ is given by

$$\mathcal{F}_t = \epsilon\mathcal{F}_{yy} - \mathcal{F}\mathcal{F}_y - \hat{p}_y; \tag{4}$$

$p(t)$ is to be determined by imposing the four boundary conditions on $\mathcal{F}$. The vorticity is given by

$$\omega = v_x - u_y = x\mathcal{F}_{yy}, \tag{5}$$

the quantity $\mathcal{F}_{yy}$ playing an important role in what follows.

3. Steady flows

3.1. Numerical results

Steady flows, for which $\mathcal{F}(y, t) = f(y)$, satisfy

$$\epsilon f'''' + f'f'' - ff''' = 0, \tag{6}$$

subject to the boundary conditions

$$f(-1) = f'(-1) = f'(1) = 0, \qquad f(1) = 1. \tag{7}$$

For values of ϵ that are not too small, the system (6–7) may readily be solved numerically. The resulting bifurcation diagram is given in Figure 1, showing $-f''(1)$, which is proportional to the shear stress at the upper channel wall, as a function of the Reynolds number R. A corresponding solution $f(y)$ for small ϵ (*i.e.* large R) is shown in Figure 2.

For the purposes of calculating numerical solutions to (6–7), it is useful to apply the following technique, due to Terrill [8], for converting the boundary-value problem (6–7) into an initial-value problem. (The technique also allows one to develop an alternative asymptotic

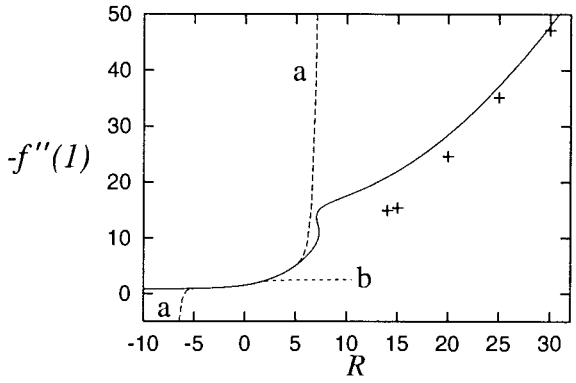

Figure 1. Solid line is a plot of $-f''(1)$ against Reynolds number $R = \epsilon^{-1}$ for numerical solutions to (6–7). Note that the solution is unique, except for a range of Reynolds numbers around $R = 7$. Where there are multiple solutions, the upper and lower branches represent temporally stable solutions to (1–2); the middle branch is unstable. Elsewhere, where the solution is unique, it is stable for $R < R_3 \approx 12{\cdot}755$, but becomes unstable in a Hopf bifurcation at $R = R_3$. The dashed line (a) shows the small-R asymptotic approximation in (11) (the plot includes terms up to R^4). When this series is reverted to give R in powers of $(f''(1) + \frac{3}{2})$, the dashed line (b) is obtained (the plot includes terms up to $(f''(1) + \frac{3}{2})^9$). Crosses show the large-R asymptotic approximation from Section 3.4, optimally truncated. For R less than around 14 it is not possible to apply this large-R approximation consistently since Equations (28) and (30) have no real solutions; it is noteworthy that this occurs fairly close to the fold.

description of f to the one given below [6, 7].) First f and y are rescaled by introducing ϕ and η through

$$f(y) = \tfrac{1}{2}\epsilon b\phi(\eta), \qquad \eta = \tfrac{1}{2}b(y+1), \tag{8}$$

where the constant b is arbitrary at this stage. The parameter ϵ is then absent from the equation for $\phi(\eta)$, which is

$$\phi_{\eta\eta\eta\eta} + \phi_\eta\phi_{\eta\eta} - \phi\phi_{\eta\eta\eta} = 0. \tag{9}$$

This equation is integrated numerically, subject to the initial conditions

$$\phi(0) = 0, \qquad \phi'(0) = 0, \qquad \phi''(0) = A, \qquad \phi'''(0) = B, \tag{10}$$

where A and B are arbitrary, until a zero of $\phi'(\eta)$, at $\eta = \bar{\eta}$, say, is obtained from the numerical calculation. By taking $b = \bar{\eta}$ we obtain from (8) a solution to the boundary-value problem (6–7); the corresponding value of ϵ is $2/(b\phi(b))$. By a suitable rescaling of ϕ and η, we may set $B = 1$. Solutions may then be calculated in the limit as $\epsilon \to 0^+$ by letting $A \to A_c^+$ [18], where $A_c \approx -1{\cdot}232$ [19].

This reformulation of the problem allows us to compute $f(y)$ for much larger Reynolds numbers than is possible by solving the full boundary-value problem (6–7) directly, for example by shooting. Since they arise as a result of the calculation, the Reynolds numbers for which we are able to compute solutions are not necessarily round numbers (this explains the 'odd' values quoted in this paper). To illustrate the practical utility of the reformulation we note that we have been able to compute $f(y)$ from (6–7) at Reynolds numbers up to around 42 by shooting from each wall and matching at an interior point, whereas we have computed f up to Reynolds numbers in the region of 10^4 using (9–10). We have checked a sample of our solutions obtained by Terrill's rescaling against direct solutions to the boundary-value

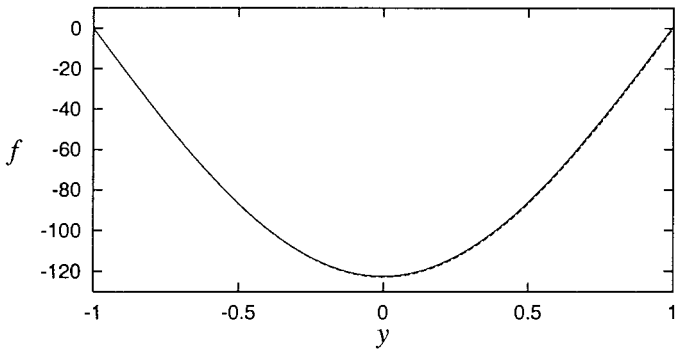

Figure 2. The solution to (6–7) for $R = 12256{\cdot}893$ (solid line), together with the leading-order outer asymptotic approximation from Section 3.4 that $f \sim -122{\cdot}909 \cos \frac{1}{2}\pi y$ (dashed line). The two lines are almost indistinguishable.

problem (6–7), where these are feasible, and have found excellent agreement. All numerical calculations were performed using integration routines from the NAG library in a double precision FORTRAN program.

In the subsections that follow we describe the asymptotic behaviour of the steady solution in the limits of small R, large wall injection ($-R \gg 1$), and large wall suction ($R \gg 1$).

3.2. STEADY FLOWS IN THE LIMIT $R \to 0$

For small Reynolds numbers, the solution to (6) may be written as a power series

$$f(y) = \sum_{n=0}^{\infty} R^n f_n(y). \tag{11}$$

The first couple of terms in this series are readily found to be $f_0(y) = \frac{1}{4}(1+y)^2(2-y)$ and $f_1(y) = -\frac{1}{1120}(1-y^2)^2(y^3+2y+35)$. From these expressions, a small-R expansion of $f''(1)$, plotted in Figure 1, is found to be $f''(1) = -\frac{3}{2} - \frac{19}{70}R + O(R^2)$. This series may readily be reverted to give R in powers of $(f''(1) + \frac{3}{2})$; the result is plotted in Figure 1. The pressure term

$$p = -\epsilon f''' - f'^2 + ff'', \tag{12}$$

has the corresponding expansion

$$Rp = \sum_{n=0}^{\infty} R^n p_n, \tag{13}$$

where the first few terms are $p_0 = 3/2$, $p_1 = -81/140$ and $p_2 = 2929/107800$.

The radius of convergence of the small-R series for p may be estimated using the extension by Mercer and Roberts [20] of the method due to Domb and Sykes [21]. We first compute a large number of terms in (13); we have computed up to $n = 36$ using the computer algebra package Maple. We then compute the quantities

$$B_n = \frac{p_{n+1}p_{n-1} - p_n^2}{p_n p_{n-2} - p_{n-1}^2} \qquad \text{and} \qquad \cos\theta_n = \frac{1}{2}\left[\frac{p_{n-1}B_n}{p_n} + \frac{p_{n+1}}{p_n B_n}\right]. \tag{14}$$

If the series in (13) has finite radius of convergence r, with convergence-limiting singularities of order q at $r\exp(\pm i\theta)$, then for large n,

$$B_n = \frac{1}{r} - \frac{1+q}{rn} + O(n^{-2}) \qquad \text{and} \qquad \cos\theta_n = \cos\theta + O(n^{-2}). \tag{15}$$

We estimate using the coefficients p_n available to us that $r \approx 5{\cdot}5$, $q \approx 0{\cdot}37$ and $\theta \approx 1{\cdot}46$, so the convergence-limiting singularities appear to lie close to the imaginary axis. Curves (a) and (b) in Figure 1 indicate the range of validity that can be obtained from the series.

3.3. Steady flows in the limit $R \to -\infty$

In the limit $R \to -\infty$, the solution to (6–7), away from a boundary layer at $y = 1$, takes the form [16]

$$f(y) \sim \cos\tfrac{\pi}{4}(1-y) - \tfrac{1}{2}(-R)^{-1/2} z_0 (\pi/4)^{1/2}(1-y)\sin\tfrac{\pi}{4}(1-y) + O((-R)^{-1}), \tag{16}$$

where the constant z_0 is to be determined by matching with the boundary-layer solution.

Near $y = -1$, f takes the form

$$f(y) \sim (-R)^{-1/2}\left\{\theta_0(\mathcal{Y}) + O((-R)^{-1/2})\right\}, \tag{17}$$

where $\mathcal{Y} = (-R)^{1/2}(y+1)$ and θ_0 satisfies

$$\theta_0'''' + \theta_0\theta_0''' - \theta_0'\theta_0'' = 0 \tag{18}$$

subject to $\theta_0(0) = \theta_0'(0) = 0$ and the matching condition $\theta_0 \sim \pi\mathcal{Y}/4$ as $\mathcal{Y} \to \infty$. Thus if we write $\theta_0(\mathcal{Y}) = (\pi/4)^{1/2}\rho(z)$, with $z = (\pi/4)^{1/2}\mathcal{Y}$, it follows that $\rho(z)$ satisfies the Falkner–Skan equation ([22], p. 316)

$$\rho''' + \rho\rho'' - \rho'^2 = -1 \tag{19}$$

(this is the case $m = 1$ in the usual notation), subject to $\rho(0) = \rho'(0) = 0$ and $\rho'(z) \sim 1$ as $z \to \infty$. Numerical evaluation of $\rho(z)$, by shooting, reveals that as $z \to \infty$, $p(z) \sim z - z_0$, where $z_0 \approx 0{\cdot}647900$ [7], and this provides the constant required in (16).

3.4. Steady flows in the limit $R \to \infty$

3.4.1. *Interior- and boundary-layer analysis*

We consider the behaviour close to $y = 1$ of solutions to (6) which satisfy

$$\text{at } y = 1 \qquad f = 1, \quad f' = 0. \tag{20}$$

We start by writing

$$y = 1 + \epsilon Y, \qquad Y < 0,$$

and define $\delta(\epsilon) \ll 1$ by taking the location of the zero of f closest to $y = 1$ to be $Y = -1/\delta$. Moreover, we define $\alpha(\epsilon) = O(1)$ and $\nu(\epsilon) \ll 1$ such that

$$\text{at } Y = -1/\delta \qquad f = 0, \qquad f_Y = \delta\alpha, \qquad f_{YYY} = -\delta^2\alpha^2\nu, \tag{21}$$

asymptotic expressions for each of the unknowns δ, α and ν being obtained below.

3.4.2. *Interior layer*
In view of (21), we scale according to

$$Y = -\frac{1}{\delta} + \frac{\hat{Y}}{(\alpha\delta)^{1/2}}, \quad f = (\alpha\delta)^{1/2}\hat{f}$$

to give

$$\begin{aligned} &\hat{f}_{\hat{Y}\hat{Y}\hat{Y}\hat{Y}} + \hat{f}_{\hat{Y}}\hat{f}_{\hat{Y}\hat{Y}} - \hat{f}\hat{f}_{\hat{Y}\hat{Y}\hat{Y}} = 0, \\ &\text{at } \hat{Y} = 0 \qquad \hat{f} = 0, \quad \hat{f}_{\hat{Y}} = 1, \quad \hat{f}_{\hat{Y}\hat{Y}\hat{Y}} = -\nu; \end{aligned} \tag{22}$$

the final condition here motivates the inclusion of the factor α^2 in the definition of ν in (21). The only parameter appearing in (22) is ν, which will prove to be exponentially small in δ (see (31) below). The first three terms in the required $\nu \to 0$ limit of (22), in which exponential growth is suppressed as $\hat{Y} \to -\infty$ (this is needed to match into the outer region), are given by

$$\hat{f} \sim \hat{Y} - \tfrac{1}{6}\nu\hat{Y}^3 + \nu^2\hat{F}, \tag{23}$$

where, writing $\hat{G} = \hat{F}_{\hat{Y}\hat{Y}\hat{Y}\hat{Y}}$, we have

$$\hat{G} \sim \hat{Y} - \sqrt{\frac{\pi}{2}}\,\mathrm{e}^{\hat{Y}^2/2}\left(1 + \mathrm{erf}\,(\hat{Y}/\sqrt{2})\right); \tag{24}$$

since

$$\hat{G} - \hat{Y}\hat{F}_{\hat{Y}\hat{Y}\hat{Y}} + \hat{F}_{\hat{Y}\hat{Y}} = -\tfrac{1}{3}\hat{Y}^3,$$

$\hat{F}$ is completely specified by integrating (24) four times using

$$\text{at } \hat{Y} = 0 \qquad \hat{F} = 0, \quad \hat{F}_{\hat{Y}} = 0, \quad \hat{F}_{\hat{Y}\hat{Y}} = \sqrt{\frac{\pi}{2}}, \quad \hat{F}_{\hat{Y}\hat{Y}\hat{Y}} = 0.$$

3.4.3. *Boundary layer $Y = O(1)$*
Writing, as $\delta \to 0$,

$$f = 1 + \delta F, \quad \alpha \sim \sum_{n=0}^{N} \delta^n \alpha_n, \quad F \sim \sum_{n=0}^{N-1} \delta^n F_n, \tag{25}$$

we have

$$\begin{aligned} &F_{nYYYY} - F_{nYYY} = \sum_{m=0}^{n-1}\left(F_m F_{(n-1-m)YYY} - F_{mY}F_{(n-1-m)YY}\right), \\ &\text{at } Y = 0 \qquad F_n = F_{nY} = 0, \\ &\text{as } Y \to -\infty \qquad F_n \sim \alpha_{n+1} + \alpha_n Y, \end{aligned} \tag{26}$$

where $\alpha_0 = 1$; here we have matched with the first term in (23), which is valid to all powers of δ. The boundary-value problem (26) determines both F_n and α_{n+1} and is readily iterated

forward in n to give closed form solutions to any desired order. The first few terms are $\alpha_1 = 1$, $\alpha_2 = 4$, $\alpha_3 = 129/4$, and $F_0(Y) = 1 + Y - \exp Y$, $F_1(Y) = 4 + Y - (\frac{1}{2}Y^2 - 3Y + 4)\exp Y$.

We note that we have been able to scale in order to formulate the above problems such that the only parameter appearing in (22) is ν and the only one in (25–26) is δ. This makes our approach both more concise and more generally applicable than previous attempts and facilitates the construction of the solution to any order in δ. At this stage of the analysis, the fact that $\nu(\epsilon)$ and $\delta(\epsilon)$ remain to be determined is not a difficulty; in solving (22) we need only to know that $\nu \ll 1$ and (25–26) is implied by $\delta \ll 1$ on the assumption (justified below) that ν is exponentially small in δ. Subsequent matching will determine δ and ν as functions of ϵ; the first stage of matching, which we now describe, relates δ to ν.

3.4.4. *Matching between interior and boundary layers*

Here we must match terms from the boundary layer which are exponentially small as $Y \to -\infty$. The important quantity in the matching is the term $-\beta_n e^Y$ in $G_n = F_{nYYYY}$, the constant β_n also being determined by solving (26); the first few terms are $\beta_0 = 1$, $\beta_1 = -2$, $\beta_2 = -\frac{9}{2}$ and $G_0(Y) = -\exp Y$, $G_1(Y) = (-\frac{1}{2}Y^2 - Y + 2)\exp Y$. Since (24) implies

$$\hat{G} \sim -\sqrt{2\pi}\, e^{\hat{Y}^2/2} \qquad \text{as } \hat{Y} \to +\infty,$$

writing

$$\beta \sim \sum_{n=0}^{N} \delta^n \beta_n \tag{27}$$

and matching requires, to any order N, that

$$\delta\beta(\delta) \sim \nu^2(\alpha(\delta)\delta)^{5/2}\sqrt{2\pi}\, e^{\alpha(\delta)/2\delta}; \tag{28}$$

hence, as promised, ν is exponentially small in δ.

3.4.5. *The outer solution*

The leading-order outer solution is simply, since the ϵ term in (6) is negligible,

$$f \sim -\frac{2\delta\alpha}{\epsilon\pi}\cos(\tfrac{1}{2}\pi y), \tag{29}$$

where we have required that to leading order (since $\delta/\epsilon \gg 1$) $f = 0$ at $y = \pm 1$ and $f' = \delta\alpha$ at $y = 1$ (to match with (23)). Matching with the second term in (23) then requires

$$\nu \sim \frac{\pi^2\epsilon^2}{4\alpha\delta}, \tag{30}$$

and (28) and (30) are the two equations determining $\delta(\epsilon)$ and $\nu(\epsilon)$, the functions $\alpha(\delta)$ and $\beta(\delta)$ being known from the analysis above. To leading order we have

$$\delta \sim \tfrac{1}{8}\log(1/\epsilon), \qquad \nu \sim 2\pi^2\epsilon^2\log(1/\epsilon) \qquad \text{as } \epsilon \to 0 \tag{31}$$

and, since the expansions proceed in powers of δ and are divergent, the use of optimal truncation methods when determining α and β (with the full balances in (28) and (30) being solved for ν and δ) typically provides the most effective way to obtain an accurate solution. The results of such a calculation are summarised in Figure 1 and Table 1.

Table 1. Comparison between the 'exact' (numerical) value of $M \equiv \max |f(y)|$, and the leading-order asymptotic approximation that $M_a = 2\alpha\delta/\pi\epsilon$. Terms up to $\alpha_{N+1}\delta^{N+1}$ and $\beta_N\delta^N$ are included in the sums used to compute α and β, where N is either 19 (the largest value of N for which we have computed α_{N+1} and β_N), or some smaller value of N, indicated in the table, which corresponds to truncating the series for β after its smallest term. For the examples given, this truncation coincides with the optimal truncation for α.

N	R	δ	α	M_a	M	Error
5	20·0	0·07331	1·1290	1·0538	1·2148	13%
5	30·0	0·05858	1·0867	1·2157	1·3404	9·3%
14	203·4503	0·03101	1·0365	4·1612	3·9662	4·9%
19	711·8385	0·02375	1·0266	11·0502	10·7866	2·4%
19	2462·234	0·01928	1·0211	30·853	30·565	0·95%
19	3572·189	0·01825	1·0198	42·314	42·018	0·71%
19	8457·171	0·01623	1·01746	88·915	88·579	0·38%
19	12256·89	0·01549	1·01660	122·909	122·495	0·34%

3.4.6. *Boundary layer at $y = -1$*

Because (29) does not satisfy $f' = 0$ at $y = -1$, a boundary layer is also needed at the left-hand (lower) boundary, but this is passive as far as the matching is concerned, the behaviour near $y = 1$ being what is crucial in governing the leading-order solution. The inner scalings are

$$y = -1 + \epsilon\bar{Y}/(\alpha\delta)^{1/2}, \qquad f = (\alpha\delta)^{1/2}\bar{F},$$

leading, on matching with (29), to the Falkner–Skan problem

$$\bar{F}_0''' + \bar{F}_0'^2 - \bar{F}_0\bar{F}_0'' = 1,$$
$$\text{at } \bar{Y} = 0 \qquad \bar{F}_0 = \bar{F}_0' = 0,$$
$$\text{as } \bar{Y} \to +\infty \qquad \bar{F}_0 \sim -\bar{Y},$$

so that $\bar{F}_0 = -\rho(\bar{Y})$ with ρ given by (19).

3.5. SUMMARY

As evidenced by Figure 1 and by the preceding discussion, asymptotic methods provide very effective means for constructing accurate analytic approximations over most of the range of Reynolds numbers. Our asymptotic analysis here has been fairly complete – we have applied regular perturbation methods for small R, together with appropriate manipulations of the resulting series (we note that treatment of the series by Padé approximants (*cf.* Drazin and Tourigny [23]) does not seem to help much in improving its convergence), together with singular perturbation methods in the limits $R \to -\infty$ and $R \to +\infty$. Our results in the limit $R \to +\infty$ are worth highlighting, being significantly more accurate than those which have been obtained before, the optimal truncation approach enabling us to obtain algebraic accuracy in ϵ despite many of the expansions proceeding in powers of $1/\log(1/\epsilon)$. Such approaches to problems involving logarithmic expansions should prove much more generally applicable and

related developments will be reported in more detail elsewhere, our main focus here being on the time-dependent problem discussed in the remaining sections.

4. Time-dependent flows: numerical results

4.1. Numerical scheme for solving the initial-value problem

Our numerical scheme for computing time-dependent flows is broadly based on one of Glenn Ierley (personal communication). Equation (1) (or in practice (3)), together with boundary conditions (2), is solved using the Chebyshev tau method [24]. We represent functions of y as sums of Chebyshev polynomials, truncated at some finite order. We find it convenient then to consider any function as being equivalent to the vector of coefficients in this finite sum. We represent numerically the solution $\mathcal{F}(y, t_n)$ at the nth time step as the vector $\boldsymbol{f}^n = (f_0^n, \ldots, f_K^n)^T$, where the superscript T denotes the transpose, with

$$\mathcal{F}(y, t_n) = \sum_{k=0}^{\infty} f_k^n T_k(y), \tag{32}$$

$T_k(y)$ being the k-th Chebyshev polynomial. Derivatives of $\mathcal{F}$ are calculated in spectral space, while products are calculated in physical space.

We discretise (3) in time as

$$\mathcal{F}_y^{n+1} - \mathcal{F}_y^{n-1} = \epsilon\Delta_t(\mathcal{F}_{yyy}^{n+1} + \mathcal{F}_{yyy}^{n-1}) + 2\Delta_t(\mathcal{F}_y^2 - \mathcal{F}\mathcal{F}_{yy} + p(t))^n, \tag{33}$$

where Δ_t is the time step and the superscript $n-1$, n or $n+1$ indicates evaluation at the corresponding time step. This expression is then readily rearranged to give an approximate equation for the Chebyshev coefficients $\boldsymbol{f}^{n+1}$ of the form

$$(D - \epsilon\Delta_t D^3)\boldsymbol{f}^{n+1} = \left[(D + \epsilon\Delta_t D^3)\boldsymbol{f}^{n-1} + 2\Delta_t \boldsymbol{g}^n\right] + (c, 0, 0, \ldots, 0)^T, \tag{34}$$

where $c = 2\Delta_t p(t_n)$ and $\boldsymbol{g}^n = (g_0^n, \ldots, g_K^n)^T$ is the vector of Chebyshev coefficients such that at the n-th time step

$$\mathcal{F}_y^2 - \mathcal{F}\mathcal{F}_{yy} = \sum_{k=0}^{\infty} g_k^n T_k(y). \tag{35}$$

The matrix D is the differentiation matrix, such that if the vector $\boldsymbol{a}$ represents the function $a(y)$ then $D\boldsymbol{a}$ represents $\mathrm{d}a/\mathrm{d}y$. In the tau method, the final three rows of the vector equation (34) are changed in order to force $\mathcal{F}^{n+1}$ to satisfy appropriate boundary conditions. Since we integrate an equation that is third-order in y, it is appropriate to apply three boundary conditions to (34); we choose to impose the homogeneous conditions from (2). To do this, the last three rows of the matrix $D - \epsilon\Delta_t D^3$ are replaced by

$$\begin{pmatrix} 1 & -1 & 1 & -1 & \cdots & (-1)^{K-1} & (-1)^K \\ 0 & -1 & 4 & -9 & \cdots & (-1)^{K-1}(K-1)^2 & (-1)^K K^2 \\ 0 & 1 & 4 & 9 & \cdots & (K-1)^2 & K^2 \end{pmatrix} \tag{36}$$

to give a modified matrix $\mathcal{D}$, and on the right-hand side of (34) the corresponding rows are replaced by zeros. The matrix $\mathcal{D}$ is then invertible, and so

$$\boldsymbol{f}^{n+1} = \mathcal{D}^{-1}\left[(D + \epsilon\Delta_t D^3)\boldsymbol{f}^{n-1} + 2\Delta_t \boldsymbol{g}^n\right]^\dagger + \mathcal{D}^{-1}(c, 0, \ldots, 0)^T, \tag{37}$$

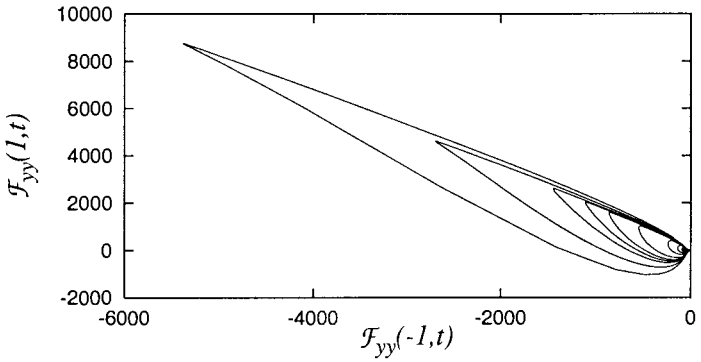

Figure 3. Limit-cycle solutions to (1–2) for $\epsilon = 0{\cdot}04$, $0{\cdot}035$, $0{\cdot}03$, $0{\cdot}025$, $0{\cdot}02$, $0{\cdot}018$, $0{\cdot}017$, $0{\cdot}016$, $0{\cdot}014$ and $0{\cdot}012$ (the cycles grow in size as ϵ decreases). Plotted are the quantities $\mathcal{F}_{yy}(-1,t)$ and $\mathcal{F}_{yy}(1,t)$, which are proportional to the wall stresses. Evolution around the limit cycle is clockwise. Note that the extreme values of $\mathcal{F}_{yy}(\pm 1,t)$ achieved around the cycle increase rapidly as ϵ is reduced.

where it is understood that the quantity $[\cdots]^\dagger$ in (37) is equal to the corresponding term in (34), modified by replacing the last three rows with zeros. At this point the quantity c is unknown, and must be determined by applying the remaining boundary condition, $\mathcal{F}(1,t_n) = 1$. Since $T_k(1) = 1$ for all k, we have

$$c = \frac{1 - \sum_{k=0}^{K} \alpha_k}{\sum_{k=0}^{K} \beta_k}, \tag{38}$$

where

$$\boldsymbol{\alpha} = \mathcal{D}^{-1}\left[(D + \epsilon\Delta_t D^3)\boldsymbol{f}^{n-1} + 2\Delta_t \boldsymbol{g}^n\right]^\dagger$$

and $\boldsymbol{\beta} = \mathcal{D}^{-1}(1,0,0,\cdots,0)^T$. This completes the evaluation of $\boldsymbol{f}^{n+1}$.

Our implementation of the numerical scheme is rather unsophisticated: for example, we use a constant time step Δ_t in each calculation, although, as we shall see, the nature of the time-dependent solutions suggests that an adaptive time-stepping algorithm would lead to a more efficient numerical solution. For each choice of ϵ, the time step Δ_t is chosen so that calculations using a smaller value of Δ_t give essentially the same results, and the numerical solution is considered to be converged.

4.2. Numerical results for the limit cycle

For $R < R_3$, the system (1–2) has at least one stable steady solution, and the numerical simulation of the initial-value problem appears to converge to a steady state at large time. The bifurcation of the steady state at $R = R_3$ is a Hopf bifurcation, at which two complex conjugate eigenvalues cross the imaginary axis. We find that the time-dependent numerical solution is attracted to the steady state for $R < R_3$ but approaches a small limit cycle for R just beyond R_3, and so we infer that the Hopf bifurcation is supercritical.

Figure 3 shows the limit cycle (by which we mean a spatially non-uniform solution that is periodic in time) for a variety of values of ϵ. It is notable that the greatest wall stresses around the limit cycle grow rapidly with decreasing ϵ. This feature of the solution makes reliable

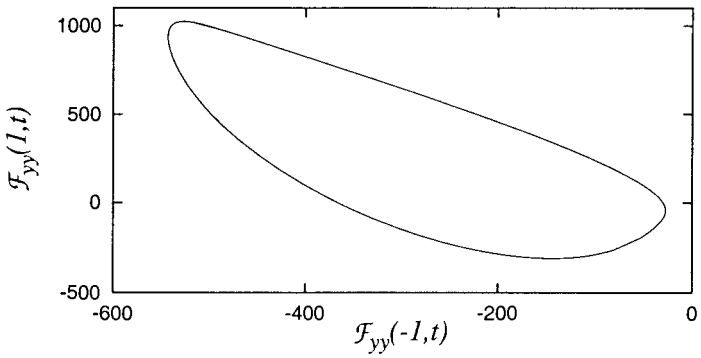

Figure 4. Limit-cycle solution to (1–2) for $\epsilon = 0{\cdot}02$. Plotted are the quantities $\mathcal{F}_{yy}(-1, t)$ and $\mathcal{F}_{yy}(1, t)$, which are proportional to the wall stresses.

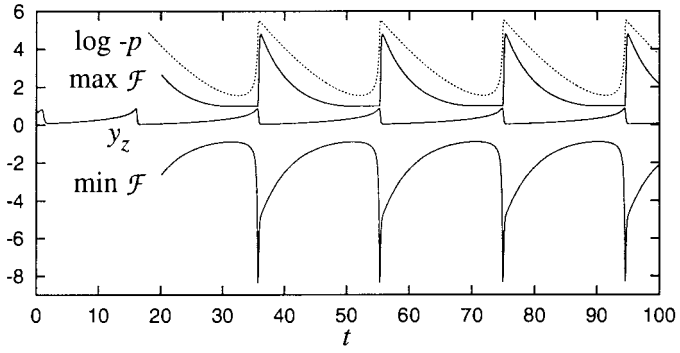

Figure 5. Time evolution of $\max_y \mathcal{F}(y, t)$, $\min_y \mathcal{F}(y, t)$, $y_z(t)$ and $\log -p(t)$ for the limit-cycle solution to (1–2) for $\epsilon = 0{\cdot}02$. Note the separation of the cycle into slow and fast phases.

computation of the solution difficult in the limit $\epsilon \to 0$. Another difficulty in computing these limit cycles for small ϵ is that evolution of $\mathcal{F}$ is extremely rapid around a small part of the limit cycle. Our method of non-adaptive time-stepping therefore becomes very inefficient in this limit.

In Figure 4 we show the limit cycle for $\epsilon = 0{\cdot}02$. More detail of this solution is shown in Figure 5, where we plot the maximum and minimum values of $\mathcal{F}(y, t)$ across the channel as functions of time. Also shown are the evolution of the pressure coefficient $p(t)$ and the interior zero $y_z(t)$ of $\mathcal{F}$, which satisfies $\mathcal{F}(y_z(t), t) = 0$ with $-1 < y_z(t) < 1$. Already for this quite moderate value of ϵ, the separation of the evolution of $\mathcal{F}(y, t)$ into slow and fast phases can clearly be discerned in Figure 5.

For small ϵ, it is a feature of the solution that the interior zero of $\mathcal{F}$ comes very close to the upper wall $y = 1$ near the start of the fast phase of the limit cycle. The zero is then swept rapidly back almost to the midline of the channel, $y = 0$. To characterise this feature, for a given limit cycle we let the minimum value of $y_z(t)$ be y_*; Figure 6 shows how y_* and $\min(1 - y_z(t))$ vary with ϵ.

4.3. PROFILES OF $\mathcal{F}(y, t)$

We now turn to the profile of $\mathcal{F}(y, t)$ during various phases of the limit cycle. To illustrate the different profiles, we show in Figure 7 the limit cycle for $\epsilon = 0{\cdot}011$, which is the smallest value

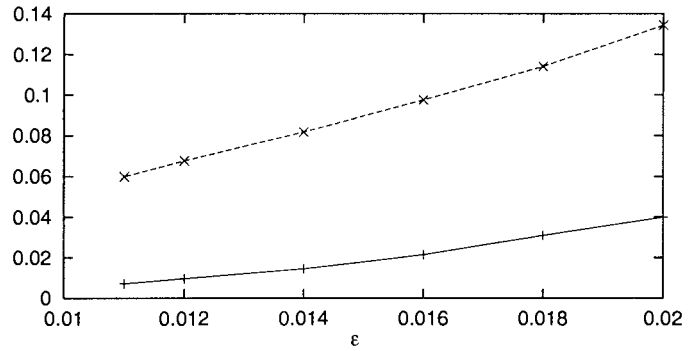

Figure 6. Lower line: plot of y_* against ϵ, where y_* is the minimum value of $y_z(t)$ over one cycle, and $\mathcal{F}(y_z(t), t) = 0$. Upper line: minimum value of $1 - y_z(t)$ over one cycle, plotted against ϵ.

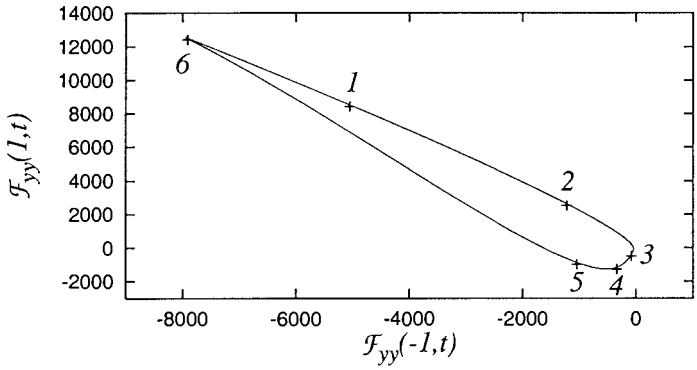

Figure 7. The limit cycle for $\epsilon = 0{\cdot}011$. The evolution of the solution from point 4 to point 6 is very rapid: for example, the time interval from point 1 to point 2 is 9 time units, while that from point 4 to point 6 is 0·15 time units. Evolution around the limit cycle is clockwise.

of ϵ for which we have reliable numerical results, and in subsequent figures the corresponding fixed-t profiles of $\mathcal{F}$.

Figure 8 shows the form of $\mathcal{F}(y, t)$ at time intervals of 0·5 between points 1 and 2 in Figure 7. Here, the solution is approximately sinusoidal away from the walls and decays

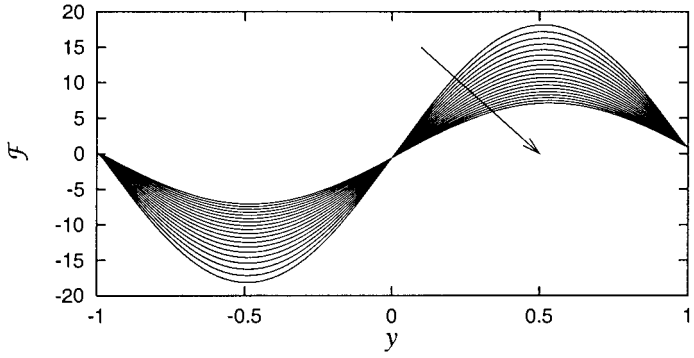

Figure 8. Profiles of $\mathcal{F}$ on the limit cycle for $\epsilon = 0{\cdot}011$. The profiles are shown at equal time intervals between points 1 and 2 in Figure 7. The arrow shows increasing t. The time interval between successive profiles is 0·5. Evolution of $\mathcal{F}$ during this phase of the limit cycle is relatively slow.

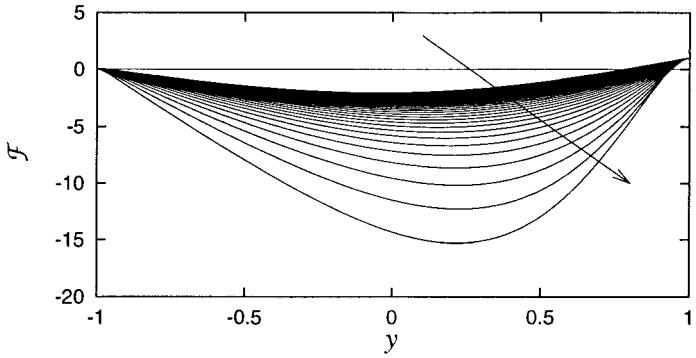

Figure 9. Profiles of $\mathcal{F}$ on the limit cycle for $\epsilon = 0{\cdot}011$. Also plotted is the y axis, for ease of identifying the interior zero of $\mathcal{F}$, $y_z(t)$. The profiles are shown at equal time intervals between points 3 and 5 in Figure 7. The arrow shows increasing t. The time interval between successive profiles is 0·01. Note the rapid evolution of $\mathcal{F}$ as y_z approaches its minimum distance from the upper wall.

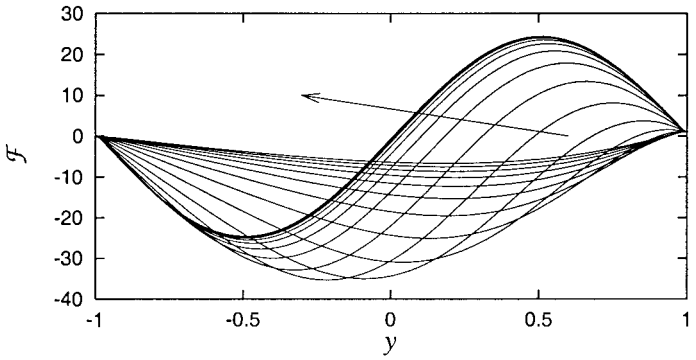

Figure 10. Profiles of $\mathcal{F}$ on the limit cycle for $\epsilon = 0{\cdot}011$. The profiles are shown at equal time intervals between points 4 and 6 in Figure 7. The arrow shows increasing t. The time interval between successive profiles is 0·01. Note the rapid evolution of $\mathcal{F}$ during this phase.

slowly. The approach of the interior zero y_z to the upper wall is illustrated in Figure 9, which shows the evolution of $\mathcal{F}$ at time intervals of 0·01 between points 3 and 5. A fast phase, during which y_z decreases almost to zero, is shown in Figure 10, where the profile of $\mathcal{F}$ is plotted at time intervals of 0·01 between points 4 and 6.

Such numerical results are very helpful in clarifying the spatio-temporal evolution of $\mathcal{F}(y, t)$ and now we turn to a small-ϵ asymptotic description of the limit cycle, restricting the analysis to solutions that are periodic in time.

5. Time-dependent flows: asymptotics of the slow phases

5.1. An exact solution

5.1.1. *Formulation*

We start this section by noting a class of exact solutions to (1); we shall subsequently explain the asymptotic relevance of the results to the boundary-value problem (1–2) in the limit $\epsilon \to 0$. The class of solutions we consider takes the form

$$\mathcal{F} = A(t) + B(t)y + C(t)\sin(\lambda(t)y) + D(t)\cos(\lambda(t)y), \tag{39}$$

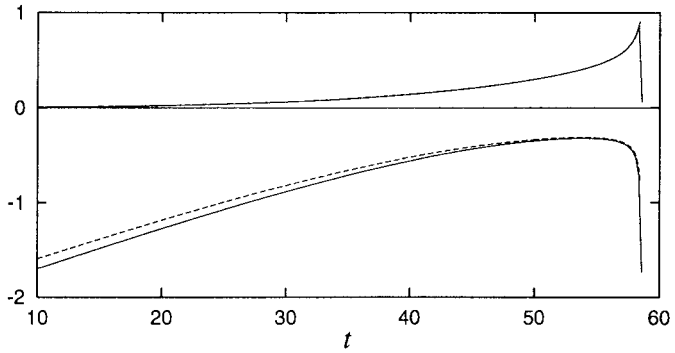

Figure 11. Comparison between asymptotics and numerics for $\epsilon = 0{\cdot}011$. The solid lines represent numerical simulations of (1–2), while the dashed lines give asymptotic results. The left- and right-hand sides of the plot correspond, respectively, to points just after and just before point 6 on Figure 7; we thus show almost a complete cycle. The upper curves show $y_z(t)$. The dashed line is the corresponding quantity calculated asymptotically by solving $\mathcal{F}(y_z(t), t) = 0$, with $\mathcal{F}(y, t)$ given in (39) or (68); the quantities A and B are given in terms of C, D and λ in (44), these last three quantities evolving according to (45). The lower curves show $-\log(-p(t))/5$, where the dashed line shows p as given in (41).

this functional form having originally been identified through its repeated occurrence when pursuing an asymptotic analysis of (1); once identified, it enables us to give a much more concise presentation of that analysis than would otherwise be the case. Equation (1) is of a quadratically nonlinear form, numerous other such systems amenable to low-dimensional reductions akin to (39) having been previously identified (see, for example, [25] and [26]). Unlike most earlier examples, however, (39) yields an underdetermined system when substituted in (1), enabling two boundary conditions to be imposed (see below; most applications of previous examples were restricted to initial-value problems). Another noteworthy feature of the current example is the appearance of a time-dependent wavelength, implying in particular the possibility of a smooth transition from trigonometric to hyperbolic functions with λ becoming imaginary on passing through zero (a scenario we shall need to make use of later).

While the reduction (39) contains five degrees of freedom, substitution in (1) leads (somewhat remarkably) to three constraints only, namely

$$\begin{aligned} \frac{\mathrm{d}\lambda}{\mathrm{d}t} &= -\lambda B, \\ \frac{\mathrm{d}C}{\mathrm{d}t} &= -\epsilon\lambda^2 C + 3BC + \lambda AD, \\ \frac{\mathrm{d}D}{\mathrm{d}t} &= -\epsilon\lambda^2 D + 3BD - \lambda AC. \end{aligned} \tag{40}$$

From (3) we have

$$\frac{\mathrm{d}B}{\mathrm{d}t} = B^2 + \lambda^2(C^2 + D^2) + p, \tag{41}$$

which gives $p(t)$ in terms of the other unknowns. It follows from (40) that

$$\frac{\mathrm{d}}{\mathrm{d}t}\left(\lambda^3(C^2 + D^2)^{1/2}\right) = -\epsilon\lambda^5(C^2 + D^2)^{1/2}, \tag{42}$$

a combination which will prove important in what follows. Because the system (40) represents only three constraints, we are able to impose two boundary conditions, the appropriate choice at this stage (for reasons indicated below) being the 'inviscid' conditions

$$\mathcal{F}(-1,t)=0, \quad \mathcal{F}(1,t)=1, \tag{43}$$

giving

$$A=\tfrac{1}{2}-D\cos\lambda, \quad B=\tfrac{1}{2}-C\sin\lambda, \tag{44}$$

and hence

$$\begin{aligned}\frac{\mathrm{d}\lambda}{\mathrm{d}t} &= -\lambda\left(\tfrac{1}{2}-C\sin\lambda\right),\\ \frac{\mathrm{d}C}{\mathrm{d}t} &= -\epsilon\lambda^2 C+3\left(\tfrac{1}{2}-C\sin\lambda\right)C+\lambda\left(\tfrac{1}{2}-D\cos\lambda\right)D,\\ \frac{\mathrm{d}D}{\mathrm{d}t} &= -\epsilon\lambda^2 D+3\left(\tfrac{1}{2}-C\sin\lambda\right)D-\lambda\left(\tfrac{1}{2}-D\cos\lambda\right)C.\end{aligned} \tag{45}$$

We shall discuss the solution to (45) subject to (for reasons which will again become clearer later)

$$\text{at } t=0 \qquad \lambda=\pi, \quad C=C_I(\epsilon), \quad D=-\tfrac{1}{2}, \tag{46}$$

where $C_I(\epsilon)\to+\infty$ as $\epsilon\to 0$ in a manner which will be determined in Section 7. A numerical solution to (45–46), together with a corresponding numerical simulation of (1–2), is given in Figure 11. We now describe the limiting behaviour of (45–46) as $\epsilon\to 0$.

5.1.2. *Slowest phases*

The results for the first (large-amplitude) phase, corresponding to solutions roughly between points 6 and 2 in Figure 7, are implicit in [15]. The appropriate scalings are (from (45))

$$t=\epsilon^{-1}\hat{T}, \quad C=C_I(\epsilon)\hat{C}, \quad \lambda\sim\pi, \quad D\sim-\tfrac{1}{2}, \tag{47}$$

it then following immediately from (42) that the leading order solution is simply

$$\hat{C}_0(\hat{T})=\mathrm{e}^{-\pi^2\hat{T}}, \tag{48}$$

with

$$\lambda(\hat{T})\sim\pi-\frac{1}{2C_I(\epsilon)\hat{C}_0} \qquad \text{as } \epsilon\to 0. \tag{49}$$

The other phase of slowest evolution corresponds to $T=O(1)$, where

$$\hat{T}=\frac{1}{\pi^2}\log(C_I(\epsilon))+T \tag{50}$$

with

$$\lambda\sim\lambda_0(T), \quad C\sim C_0(T), \quad D\sim D_0(T) \qquad \text{as } \epsilon\to 0,$$

so that (from (42) and (45))

$$C_0\sin\lambda_0=\tfrac{1}{2}, \qquad D_0\cos\lambda_0=\tfrac{1}{2}, \tag{51}$$

and

$$\frac{\mathrm{d}}{\mathrm{d}T}\left(\frac{\lambda_0^3}{\sin 2\lambda_0}\right) = -\frac{\lambda_0^5}{\sin 2\lambda_0}, \qquad (52)$$
$$\text{as } T \to -\infty \quad \lambda_0 \sim \pi - \tfrac{1}{2}\mathrm{e}^{\pi^2 T},$$

where we have matched with (49); we note that $\sin 2\lambda_0 < 0$. We have

$$p \sim -\left(\frac{4\lambda_0}{\sin 2\lambda_0}\right)^2.$$

It follows from (52) that λ_0 decreases monotonically until it reaches $\lambda_0 = \lambda_c$, where

$$3\tan 2\lambda_c = 2\lambda_c, \qquad \lambda_c \approx 2{\cdot}039, \qquad (53)$$

at which point the solution suffers finite-time breakdown, with

$$\lambda \sim \lambda_c + \frac{\lambda_c^2}{(2\lambda_c^2+3)^{1/2}}(T_{c0} - T)^{1/2} \qquad \text{as } T \to T_{c0}^- \qquad (54)$$

for some T_{c0}. This breakdown of the solution to (52) leads on to a sequence of increasingly shorter timescales and we now describe the first of these.

5.1.3. *Intermediate phase*

The appropriate scalings here are

$$T = T_c(\epsilon) + \epsilon^{2/3}\tau, \qquad \lambda = \lambda_c + \epsilon^{1/3}\Lambda, \qquad (55)$$

where $T_c(0) = T_{c0}$, and

$$C = \frac{1}{2\sin\lambda} + \epsilon^{2/3}c, \qquad D = \frac{1}{2\cos\lambda} + \epsilon^{2/3}d. \qquad (56)$$

The prediction of much faster evolution when λ reaches the particular value λ_c is noteworthy. To leading order, (45) yields only two independent constraints, but a third is provided at once by (42) (which thus acts as a solvability condition), giving the system

$$\frac{\mathrm{d}\Lambda_0}{\mathrm{d}\tau} = \lambda_c \sin\lambda_c\, c_0, \qquad \frac{\mathrm{d}\Lambda_0}{\mathrm{d}\tau} = \lambda_c \cos\lambda_c\, d_0,$$
$$\frac{2(2\lambda_c^2+3)}{\sin 2\lambda_c}\Lambda_0\frac{\mathrm{d}\Lambda_0}{\mathrm{d}\tau} + \lambda_c^2\left(\cos\lambda_c\frac{\mathrm{d}c_0}{\mathrm{d}\tau} + \sin\lambda_c\frac{\mathrm{d}d_0}{\mathrm{d}\tau}\right) = -\frac{\lambda_c^4}{\sin 2\lambda_c}. \qquad (57)$$

Matching back as $\tau \to -\infty$ we have, by suitable choice of the origin of τ in (55),

$$\sin\lambda_c\, c_0 = \cos\lambda_c\, d_0, \qquad \frac{2\lambda_c^2+3}{2\sin\lambda_c}\Lambda_0^2 + \lambda_c^2 c_0 = \frac{\lambda_c^4}{2\sin\lambda_c}(-\tau) \qquad (58)$$

and

$$\frac{\mathrm{d}\Lambda_0}{\mathrm{d}\tau} = \frac{1}{2\lambda_c}\left(\lambda_c^4(-\tau) - (2\lambda_c^2+3)\Lambda_0^2\right), \qquad (59)$$

so that

$$\Lambda_0 = \frac{2\lambda_c}{(2\lambda_c^2+3)}\frac{\mathrm{d}}{\mathrm{d}\tau}\left(\log\left(\mathrm{Ai}\left(\left(\frac{\lambda_c^2(2\lambda_c^2+3)}{4}\right)^{1/3}(-\tau)\right)\right)\right). \tag{60}$$

It follows from (59) that

$$\Lambda_0 \sim -\frac{2\lambda_c}{(2\lambda_c^2+3)}\frac{1}{(\tau_{c0}-\tau)} \qquad \text{as } \tau \to \tau_{c0}^- \tag{61}$$

for some τ_{c0} which can be expressed using (60) in terms of the first zero of the Airy function. This blow-up in the current formulation requires consideration of the next (and final) phase of this section, during which viscous effects play no role at leading order.

5.1.4. *Inviscid phase*
We write

$$\tau = \tau_c(\epsilon) + \epsilon^{1/3}\hat{t}, \tag{62}$$

where $\tau_c(0) = \tau_{c0}$, and let

$$\lambda \sim \lambda_0(\hat{t}), \quad C \sim C_0(\hat{t}), \quad D \sim D_0(\hat{t}) \qquad \text{as } \epsilon \to 0,$$

these functions being distinct from those which appeared in Section 5.1.2. In (45) it is then only the viscous terms that are negligible, so that

$$\begin{aligned}
\frac{\mathrm{d}\lambda_0}{\mathrm{d}\hat{t}} &= -\lambda_0\left(\tfrac{1}{2} - C_0\sin\lambda_0\right),\\
\frac{\mathrm{d}C_0}{\mathrm{d}\hat{t}} &= 3\left(\tfrac{1}{2} - C_0\sin\lambda_0\right)C_0 + \lambda_0\left(\tfrac{1}{2} - D_0\cos\lambda_0\right)D_0,\\
\frac{\mathrm{d}D_0}{\mathrm{d}\hat{t}} &= 3\left(\tfrac{1}{2} - C_0\sin\lambda_0\right)D_0 - \lambda_0\left(\tfrac{1}{2} - D_0\cos\lambda_0\right)C_0,
\end{aligned} \tag{63}$$

subject to $\lambda_0 \to \lambda_c$, $C_0 \to \frac{1}{2}\sin\lambda_c$, $D_0 \to \frac{1}{2}\cos\lambda_c$ as $\hat{t} \to -\infty$, implying that

$$\lambda_0^3(C_0^2 + D_0^2)^{1/2} = \lambda_c^3/(-\sin 2\lambda_c), \tag{64}$$

a constant (*cf.* (42)). The solution to (63) also suffers finite-time blow-up at $\hat{t} = \hat{t}_{c0}$, say, with

$$C_0 \sim \frac{\lambda_c^3}{\lambda_0^3\sin 2\lambda_c}, \quad D \sim \frac{D_c}{\lambda_0^2}, \tag{65}$$

for some constant D_c, and

$$\lambda_0 \sim \left(\frac{2\lambda_c^3}{-\sin 2\lambda_c}\right)^{1/2}\left(\hat{t}_{c0} - \hat{t}\right)^{1/2} \qquad \text{as } \hat{t} \to \hat{t}_{c0}^-. \tag{66}$$

It follows from (39), (44) that at $\hat{t} = \hat{t}_c$

$$\mathcal{F} \sim \tfrac{1}{2}(1+y) + \tfrac{1}{2}D_c(1-y^2) - \tfrac{1}{6}C_c y(1-y^2), \tag{67}$$

where $C_c = \lambda_c^3/(-\sin 2\lambda_c)$. In terms of the solution to the inviscid RPJ equation, the apparent singularity in (65–66) is thus illusory; in other words, there is no breakdown in the partial

differential equation itself but only in the *ansatz* needed to describe its solution, which ceases to be of the form (39) and becomes

$$\mathcal{F} = A(t) + B(t)y - \Gamma(t)\sinh(\mu(t)y) + D(t)\cosh(\mu(t)y), \tag{68}$$

which corresponds to setting $\lambda = \mathrm{i}\mu$, $C = \mathrm{i}\Gamma$ in (39), the asymptotic solution shown in Figure 11 having been constructed by solving (45) numerically for $t < t_c$ and the analogous system for (68–69) for $t > t_c$, proceeding through $t = t_c$ via (67); blow-up behaviour of the form (65–66) applies to the full system (45) as well as to the $\epsilon \to 0$ limit. We now have

$$A = \tfrac{1}{2} - D\cosh\mu, \quad B = \tfrac{1}{2} + \Gamma\sinh\mu \tag{69}$$

and, instead of (63),

$$\begin{aligned}
\frac{\mathrm{d}\mu_0}{\mathrm{d}\hat{t}} &= -\mu_0\left(\tfrac{1}{2} + \Gamma_0\sinh\mu_0\right), \\
\frac{\mathrm{d}\Gamma_0}{\mathrm{d}\hat{t}} &= 3\left(\tfrac{1}{2} + \Gamma_0\sinh\mu_0\right)\Gamma_0 + \mu_0\left(\tfrac{1}{2} - D_0\cosh\mu_0\right)D_0, \\
\frac{\mathrm{d}D_0}{\mathrm{d}\hat{t}} &= 3\left(\tfrac{1}{2} + \Gamma_0\sinh\mu_0\right)D_0 + \mu_0\left(\tfrac{1}{2} - D_0\cosh\mu_0\right)\Gamma_0,
\end{aligned} \tag{70}$$

with, in place of (64),

$$\mu_0^3\left(\Gamma_0^2 - D_0^2\right)^{1/2} = \lambda_c^3/(-\sin 2\lambda_c). \tag{71}$$

Initial conditions on (70) are

$$\mu_0 \sim \left(\frac{2\lambda_c^3}{-\sin 2\lambda_c}\right)\left(\hat{t} - \hat{t}_{c0}\right)^{1/2} \qquad \text{as } \hat{t} \to \hat{t}_{c0}^{+}$$

with

$$\Gamma_0 \sim \frac{\lambda_c^3}{\mu_0^3\sin 2\lambda_c}, \qquad D \sim -\frac{D_c}{\mu_0^2}.$$

The solution to (70) blows up in finite time, at $\hat{t} = \hat{t}_{b0}$ say, and we need to describe this blow-up behaviour in some detail. As $\hat{t} \to \hat{t}_{b0}^{-}$, we have $\mu_0 \to +\infty$ with $\Gamma_0 \sim -D_0$ so that

$$\frac{\mathrm{d}\mu_0}{\mathrm{d}\hat{t}} \sim \tfrac{1}{2}\mu_0 D_0 \mathrm{e}^{\mu_0}, \qquad \frac{\mathrm{d}D_0}{\mathrm{d}\hat{t}} \sim \tfrac{1}{2}\mu_0 D_0^2\mathrm{e}^{\mu_0} - \tfrac{3}{2}D_0^2\mathrm{e}^{\mu_0}, \tag{72}$$

from which it follows that

$$D_0 \sim D_b\mu_0^{-3}\mathrm{e}^{\mu_0}$$

for some constant D_b and hence that as $\hat{t} \to \hat{t}_{b0}^{-}$,

$$\begin{aligned}
\mu_0 &\sim -\tfrac{1}{2}\log(\hat{t}_{b0} - \hat{t}) + \log(-\log(\hat{t}_{b0} - \hat{t})) - \tfrac{1}{2}\log D_b - \log 2, \\
D_0 &\sim \frac{4D_b^{1/2}}{(\hat{t}_{b0} - \hat{t})^{1/2}(-\log(\hat{t}_{b0} - \hat{t}))^2}.
\end{aligned} \tag{73}$$

The asymptotic behaviour of

$$\mathcal{F}_0 = \left(\tfrac{1}{2} - D_0 \cosh \mu_0\right) + \left(\tfrac{1}{2} + \Gamma_0 \sinh \mu_0\right) y - \Gamma_0 \sinh(\mu_0 y) + D_0 \cosh(\mu_0 y) \tag{74}$$

therefore subdivides into three regions as $\hat{t} \to \hat{t}_{b0}^-$, as follows.
(I) $y = O(1)$ with $y < 1$.

$$\mathcal{F}_0 \sim -\frac{1}{(\hat{t}_{b0} - \hat{t})(-\log(\hat{t}_{b0} - \hat{t}))}(1 + y). \tag{75}$$

(II) $1 - y = O(1/(-\log(\hat{t}_{b0} - \hat{t})))$.

$$\mathcal{F}_0 \sim -\frac{2}{(\hat{t}_{b0} - \hat{t})(-\log(\hat{t}_{b0} - \hat{t}))}\left(1 - \exp(\log(\hat{t}_{b0} - \hat{t})(1 - y)/2)\right). \tag{76}$$

(III) $1 - y = O(\hat{t}_{b0} - \hat{t})$.

$$\mathcal{F}_0 \sim 1 - \frac{1 - y}{\hat{t}_{b0} - \hat{t}}, \tag{77}$$

so that the interior zero of $\mathcal{F}$ satisfies

$$y_z \sim 1 - (\hat{t}_{b0} - \hat{t}) \qquad \text{as } \hat{t} \to \hat{t}_{b0}^-. \tag{78}$$

It is noteworthy that none of these leading-order expressions depends on D_b.

Unlike (65–66), this form of singularity in the solution is genuine, rather than simply reflecting a straightforward change in the appropriate representation of the solution. In other words, when $\hat{t}$ becomes sufficiently close to $\hat{t}_{b0}$, the *ansatz* (68) ceases to apply and a quite different approach is needed. We discuss the behaviour of this next phase in Section 6. Having been of $O(1)$ for $\hat{t} = O(1)$ (during which it reaches its minimum value), $-p$ blows up as $\hat{t}_{b0}$ is approached (*cf.* Figure 11) according to

$$p \sim -\frac{1}{(\hat{t}_{b0} - \hat{t})^2(-\log(\hat{t}_{b0} - \hat{t}))^2} \qquad \text{as } \hat{t} \to \hat{t}_{b0}^-. \tag{79}$$

5.2. Other regions

5.2.1. *Preliminaries*

The solution (39), (68), subject to (43), provides an asymptotic description of the behaviour away from the boundary layers at $y = \pm 1$. The purpose of the current subsection is to describe these boundary layers and to indicate why the interior layer located about the zero of $\mathcal{F}$ (which played such a crucial role in Section 3.4) does not need separate treatment here. The other issue which needs to be resolved in order to demonstrate the applicability of (39) concerns the initial data; it is necessary for the above reduction to be valid that (39), (44) (together with (46)) apply to leading order at $t = 0$. Since we are seeking solutions which are periodic in time, this is a point to which we shall have to return at the end of the analysis.

It is instructive to note next the balances in (1) which correspond to the various timescales in Section 5.1. On the slow timescales of Section 5.1.2, the dominant balance is inviscid and quasi-steady; from

$$\epsilon \mathcal{F}_{yyT} = \epsilon \mathcal{F}_{yyyy} + \mathcal{F}_y \mathcal{F}_{yy} - \mathcal{F} \mathcal{F}_{yyy} \tag{80}$$

we have at leading order

$$\mathcal{F}_{0y}\mathcal{F}_{0yy} - \mathcal{F}_0\mathcal{F}_{0yyy} = 0, \tag{81}$$

so, imposing (43), we find

$$\mathcal{F}_0 = \frac{\sin\lambda_0(T)(y+1)}{\sin 2\lambda_0(T)}; \tag{82}$$

the quantity $\lambda_0(T)$ is not determined by the inviscid balance (81) but requires consideration of the interior layer (as outlined below); its calculation is automatically included in the analysis of (39) because the *ansatz* encompasses both the outer regions $y = O(1)$, $-1 < y < y_z$ and $y_z < y < 1$, and the viscous interior layer about $y = y_z$.

The timescale of Section 5.1.3 is the one for which the use of the *ansatz* (39) leads to the greatest gain in brevity; basing the discussion on (1) instead would require the consideration of the first two correction terms to the leading-order outer solution

$$\mathcal{F}_0 = \frac{\sin\lambda_c(y+1)}{\sin 2\lambda_c},$$

which is independent of τ, together with their matching into the interior layer. Corresponding to Section 5.1.4, we have the inviscid leading-order balance

$$\mathcal{F}_{0y\hat{t}} = \mathcal{F}_{0y}\mathcal{F}_{0yy} - \mathcal{F}_0\mathcal{F}_{0yyy}, \tag{83}$$

$$\mathcal{F}_0(-1,\hat{t}) = 0, \quad \mathcal{F}_0(1,\hat{t}) = 1. \tag{84}$$

Two boundary conditions are sufficient here, despite (83) being third order in y; as explained in [15] (see also Appendix A.1), (83) has partly hyperbolic nature, with characteristic projections given by

$$\frac{\mathrm{d}y}{\mathrm{d}\hat{t}} = \mathcal{F}_0$$

and, because of (84), these carry information out of the fluid domain (in other words, the conditions (84) and the initial data are sufficient to determine $\mathcal{F}_0$, no new characteristics being generated at the boundaries). A crucial (and rather delicate) issue later will be to find balances whereby information is propagated back into the fluid from a viscous boundary layer (were this not possible the blow-up in (75–77) could not be obviated, because viscous effects could not influence (83), the solution to which suffers blow-up at $\hat{t} = \hat{t}_{b0}$).

We are now in a position to discuss the two boundary layers and the interior layer.

5.2.2. *Boundary layer at $y = -1$*
If we write $\mathcal{F} = \epsilon^{1/2}\bar{\mathcal{G}}$, $y = -1 + \epsilon^{1/2}\bar{Y}$, Equation (80) yields for $T = O(1)$

$$\begin{aligned}
&\bar{\mathcal{G}}_{0\bar{Y}\bar{Y}\bar{Y}\bar{Y}} + \bar{\mathcal{G}}_{0\bar{Y}}\bar{\mathcal{G}}_{0\bar{Y}\bar{Y}} - \bar{\mathcal{G}}_0\bar{\mathcal{G}}_{0\bar{Y}\bar{Y}\bar{Y}} = 0,\\
&\text{at } \bar{Y} = 0 \qquad \bar{\mathcal{G}}_0 = \bar{\mathcal{G}}_{0\bar{Y}} = 0,\\
&\text{as } \bar{Y} \to +\infty \qquad \bar{\mathcal{G}}_0 \sim \mathcal{F}_{0y}(-1,T)\bar{Y},
\end{aligned}$$

where $\mathcal{F}_0$ is given by (82). The scalings

$$\bar{\mathcal{G}}_0 = \left(-\mathcal{F}_{0y}(-1,T)\right)^{1/2}\bar{q}(\bar{\xi}), \quad \bar{Y} = \left(-\mathcal{F}_{0y}(-1,T)\right)^{-1/2}\bar{\xi}$$

reduce this to a standard Falkner–Skan problem (*cf.* Section 3.3 above and Section 3 of [7]).

For $\hat{t} = O(1)$ we obtain the full balance in (1), with

$$\begin{aligned} &\bar{\mathcal{G}}_{0\bar{Y}\bar{Y}\hat{t}} = \bar{\mathcal{G}}_{0\bar{Y}\bar{Y}\bar{Y}\bar{Y}} + \bar{\mathcal{G}}_{0\bar{Y}}\bar{\mathcal{G}}_{0\bar{Y}\bar{Y}} - \bar{\mathcal{G}}_0\bar{\mathcal{G}}_{0\bar{Y}\bar{Y}\bar{Y}}, \\ &\text{at } \bar{Y} = 0 \qquad \bar{\mathcal{G}}_0 = \bar{\mathcal{G}}_{0\bar{Y}} = 0, \\ &\text{as } \bar{Y} \to +\infty \qquad \bar{\mathcal{G}}_0 \sim \mathcal{F}_{0y}(-1, \hat{t})\bar{Y}, \end{aligned} \tag{85}$$

where $\mathcal{F}_0$ is the solution to (83–84). Little more can usefully be said about (85); its solution does not in any case influence the behaviour elsewhere. The other timescales of Section 5.1 do not warrant separate discussion.

5.2.3. *Boundary layer at $y = 1$*

From

$$\mathcal{F} = 1 + \epsilon\mathcal{G}, \quad y = 1 + \epsilon Y \tag{86}$$

we find, on any of the timescales of Section 5.2,

$$\begin{aligned} &\mathcal{G}_{0YYYY} - \mathcal{G}_{0YYY} = 0, \\ &\text{at } Y = 0 \qquad \mathcal{G}_0 = \mathcal{G}_{0Y} = 0, \\ &\text{as } Y \to -\infty \qquad \mathcal{G}_0 \sim \mathcal{F}_{0y}\big|_{y=1} Y, \end{aligned}$$

so that

$$\mathcal{G}_0 = \mathcal{F}_{0y}\big|_{y=1} \left(Y + 1 - \mathrm{e}^Y\right). \tag{87}$$

5.2.4. *Interior layer at $y = y_z$*

With the interior zero of $\mathcal{F}$ at $y = y_z(t; \epsilon)$, for $T = O(1)$ the inner scalings are

$$y = y_z(T; \epsilon) + \epsilon^{1/2} z, \quad \mathcal{F} = \epsilon^{1/2} g, \tag{88}$$

giving a balance in which the viscous term appears at leading order, namely

$$\epsilon g_{zzT} - \epsilon^{1/2} \frac{\mathrm{d}y_z}{\mathrm{d}T} g_{zzz} = g_{zzzz} + g_z g_{zz} - g g_{zzz}. \tag{89}$$

From (82) we have

$$y_z(T; 0) = \frac{\pi}{\lambda_0} - 1 \equiv y_{z0}$$

and

$$\mathcal{F}_0 = \mathcal{F}_{0yy} = \mathcal{F}_{0yyyy} = 0 \qquad \text{at } y = y_{z0}(T),$$

so if in (89) we write

$$g \sim g_0 + \epsilon^{1/2} g_1 + \epsilon g_2 + \epsilon^{3/2} g_3 + \epsilon^2 g_4$$

we obtain

$$\begin{aligned} g_0 = \mathcal{F}_{0y}(y_{z0}, T) z, \quad g_1 = \alpha_1(T) z, \quad g_2 = \alpha_2(T) z + \tfrac{1}{6} \mathcal{F}_{0yyy}(y_{z0}, T) z^3, \\ g_3 = \alpha_3(T) z - \tfrac{1}{2} \frac{\mathrm{d}y_{z0}}{\mathrm{d}T} \frac{\mathcal{F}_{0yyy}(y_{z0}, T)}{\mathcal{F}_{0y}(y_{z0}, T)} z^2 + \beta_3(T) z^3, \end{aligned} \tag{90}$$

where the calculation of α_1, α_2, α_3 and β_3 would require the construction of correction terms to the outer solution; they need not concern us here. The crucial equation arises from the z derivative of (89) at $O(\epsilon^2)$, giving

$$G_{4z} - \mathcal{F}_{0y}(y_{z0}, T) z G_4 = g_{2zzzT} - g_{2zz}^2 = \frac{\mathrm{d}}{\mathrm{d}T}\left(\mathcal{F}_{0yyy}(y_{z0}, T)\right) - \mathcal{F}_{0yyy}^2(y_{z0}, T) z^2, \qquad (91)$$

where $G_4 = g_{4zzzz}$. Since G_4 is required not to grow exponentially as $|z| \to \infty$, we obtain from (91) that

$$G_4 = \frac{\mathcal{F}_{0yyy}^2(y_{z0}, T)}{\mathcal{F}_{0y}(y_{z0}, T)} z$$

together with the solvability condition

$$\frac{\mathrm{d}}{\mathrm{d}T}\left(\mathcal{F}_{0yyy}(y_{z0}, T)\right) = \frac{\mathcal{F}_{0yyy}^2(y_{z0}, T)}{\mathcal{F}_{0y}(y_{z0}, T)}; \qquad (92)$$

since

$$\mathcal{F}_{0y}(y_{z0}, T) = -\frac{\lambda_0}{\sin 2\lambda_0}, \quad \mathcal{F}_{0yyy}(y_{z0}, T) = \frac{\lambda_0^3}{\sin 2\lambda_0}$$

we thus recover (52), thereby completely specifying the outer solution (82).

There are two important points to make about the above. The first is that at each order the inner solution is simply a polynomial in z, so the upshot of the inner analysis (*i.e.* of the effects of viscosity) is that the outer solution is required at each order to be analytic at $y = y_{z0}$; given this constraint, (92) can instead be derived solely by consideration of the outer expansion. Secondly, the time derivative in (91) is crucial in suppressing exponential growth via the solvability condition (92). As is implicit in Section 3.4, in the steady-state problem exponential growth cannot in general be eliminated in an interior layer about a zero of f at which $f_y > 0$ and this feature is crucial in showing that the interior layer described in Section 3.4.2 must lie close to $y = 1$. By contrast, in the time-dependent problem y_z can be placed anywhere, but must evolve in a way which suppresses the exponential growth that would otherwise be present (namely, according to (92)).

The above solvability condition can be viewed as arising from the viscous effects in the interior layer. The situation for $\hat{t} = O(1)$ is rather different, the interior layer being passive as far as the matching is concerned, viscous effects playing no role in the solution to (83–84). In this case the inner scalings are

$$y = y_z(\hat{t}; \epsilon) + \epsilon\hat{z}, \qquad \mathcal{F} = \epsilon\hat{g}$$

with

$$\epsilon\hat{g}_{\hat{z}\hat{z}\hat{t}} - \frac{\mathrm{d}y_z}{\mathrm{d}\hat{t}}\hat{g}_{\hat{z}\hat{z}\hat{z}} = \hat{g}_{\hat{z}\hat{z}\hat{z}\hat{z}} + \epsilon(\hat{g}_{\hat{z}}\hat{g}_{\hat{z}\hat{z}} - \hat{g}\hat{g}_{\hat{z}\hat{z}\hat{z}}). \qquad (93)$$

Hence at each order one has

$$\hat{g}_{n\hat{z}\hat{z}\hat{z}\hat{z}} + \frac{\mathrm{d}y_{z0}}{\mathrm{d}\hat{t}}\hat{g}_{n\hat{z}\hat{z}\hat{z}} = \text{ polynomial in } \hat{z},$$

which itself has a polynomial solution and does not lead to a solvability condition. The corresponding equation for (89) reads

$$g_{nzzzz} + \mathcal{F}_{0y}(y_{z0}, T)g_{nzz} - \mathcal{F}_0(y_{z0}, T)zg_{nzzz} = \text{ polynomial in } z,$$

a solvability condition on the right-hand side arising at each order on requiring that g_n be a polynomial (or, equivalently, that exponential growth be absent) because the left-hand side vanishes for $g_n = z^3$.

This completes our description of the slower phases of evolution, which can be described most concisely via (39) and (68). We shall shortly see that a similar expression (see (154)) plays an important role during one of the faster phases, though the first (and most important) of these, discussed next, requires a quite different approach.

6. Time-dependent flows: the phases of closest approach

6.1. Formulation

The results (77–78) and (86–87) each indicate that the preceding analysis breaks down on the timescale $\hat{T} = O(1)$, where

$$\hat{t} = \hat{t}_b(\epsilon) + \epsilon\hat{T}, \tag{94}$$

with $\hat{t}_b(0) = \hat{t}_{b0}$. On this timescale we have at leading order

$$\begin{aligned}
&\mathcal{F}_{0Y\hat{T}} = \mathcal{F}_{0YYY} + \mathcal{F}_{0Y}^2 - \mathcal{F}_0\mathcal{F}_{0YY},\\
&\text{at } Y = 0 \qquad \mathcal{F}_0 = 1, \quad \mathcal{F}_{0Y} = 0,\\
&\text{as } Y \to -\infty \qquad \mathcal{F}_0 \sim Y/(-\hat{T}),\\
&\text{as } \hat{T} \to -\infty \qquad \begin{cases} \mathcal{F}_0 \sim 1 + (Y + 1 - \mathrm{e}^Y)/(-\hat{T}) & \text{for } Y = O(1),\\ \mathcal{F}_0 \sim 1 + Y/(-\hat{T}) & \text{for } Y = O(-\hat{T}), \end{cases}
\end{aligned} \tag{95}$$

where we have matched with (77) and (87). The initial–boundary-value problem (95) is a crucial one, describing the manner in which viscous effects serve to reduce the rate at which the interior zero approaches the right-hand boundary, y_z achieving its closest approach to $y = 1$ (whereby $1 - y_z = O(\epsilon)$) on this timescale.

The formulation (95) is the one of most significance for $\hat{T} = O(1)$ and is discussed is Sections 6.2–6.4 below; the scalings which apply on this timescale in the other regions are as follows.

(A) $Y = \hat{Y}/\epsilon\log(1/\epsilon), \quad \mathcal{F} = \hat{\mathcal{F}}/\epsilon\log(1/\epsilon),$
giving

$$\begin{aligned}
&\hat{\mathcal{F}}_{0\hat{Y}\hat{T}} = \hat{\mathcal{F}}_{0\hat{Y}}^2 - \hat{\mathcal{F}}_0\hat{\mathcal{F}}_{0\hat{Y}\hat{Y}},\\
&\text{at } \hat{Y} = 0 \qquad \hat{\mathcal{F}}_0 = 0,\\
&\text{as } \hat{Y} \to -\infty \qquad \hat{\mathcal{F}}_{0\hat{Y}} \to 0,\\
&\text{as } \hat{T} \to -\infty \qquad \hat{\mathcal{F}}_0 \sim -2(1 - \mathrm{e}^{\hat{Y}/2})/(-\hat{T}),
\end{aligned} \tag{96}$$

where we have matched with (76); the solution to (96) is separable, giving

$$\hat{\mathcal{F}}_0 = -2(1 - \mathrm{e}^{\hat{Y}/2})/(-\hat{T}). \tag{97}$$

(B) $y = O(1), \quad \hat{\mathcal{F}} \sim \tilde{\mathcal{F}}_0(y, \hat{T})$,
implying

$$\tilde{\mathcal{F}}_{0y\hat{T}} = 0, \tag{98}$$

so imposing $\tilde{\mathcal{F}}_0 = 0$ on $y = -1$ and matching with (75) and (97), we find

$$\tilde{\mathcal{F}}_0 = -(1+y)/(-\hat{T}). \tag{99}$$

The pressure coefficient is determined by this region, giving

$$p \sim -\frac{1}{\epsilon^2 \log^2(1/\epsilon)(-\hat{T})^2}.$$

(C) $y = -1 + \epsilon\bar{y}, \quad \mathcal{F} = \hat{\mathcal{G}}/\log(1/\epsilon)$,
where, at leading order,

$$\begin{aligned} &\hat{\mathcal{G}}_{0\bar{y}\bar{y}\hat{T}} = \hat{\mathcal{G}}_{0\bar{y}\bar{y}\bar{y}\bar{y}} \\ &\text{at } \bar{y} = 0 \qquad \hat{\mathcal{G}}_0 = \hat{\mathcal{G}}_{0\bar{y}} = 0, \\ &\text{as } \bar{y} \to +\infty \qquad \hat{\mathcal{G}}_0 \sim -\bar{y}/(-\hat{T}); \end{aligned} \tag{100}$$

initial conditions on (100) as $\hat{T} \to -\infty$ must be deduced from the behaviour of (85) as $\hat{t} \to \hat{t}_{b0}^-$, namely

$$\bar{\mathcal{G}}_0 \sim \frac{1}{\left(\hat{t}_{b0} - \hat{t}\right)^{1/2}\left(-\log\left(\hat{t}_{b0} - \hat{t}\right)\right)} \Phi\left(\frac{\bar{Y}}{\left(\hat{t}_{b0} - \hat{t}\right)^{1/2}}\right) \tag{101}$$

with

$$\Phi(\eta) = -\eta + \sqrt{\pi}\left(1 - \mathrm{e}^{\eta^2/4}\mathrm{erfc}\,(\eta/2)\right), \tag{102}$$

the nonlinear terms in (85) being negligible. From this it follows that the required solution to (100) is

$$\hat{\mathcal{G}}_0 = \frac{1}{(-\hat{T})^{1/2}} \Phi\left(\frac{\bar{y}}{(-\hat{T})^{1/2}}\right), \tag{103}$$

with $\Phi(\eta)$ again given by (102).

We now return to (95), the most important feature of which is its behaviour in the limit $\hat{T} \to 0^-$; however, to obtain a sufficiently complete description of this we must first analyse the limits $\hat{T} \to -\infty$ and $Y \to -\infty$, considering an exponentially small correction term to

$$\mathcal{F}_0 \sim Y/(-\hat{T}) + Y_\infty(\hat{T}) \qquad \text{as } Y \to -\infty \tag{104}$$

where Y_∞ is determined as part of the solution to (95).

6.2. The limit $\hat{T} \to -\infty$

In (104), it follows from (95) that

$$Y_\infty(\hat{T}) \sim 1 + 1/(-\hat{T}) \qquad \text{as } \hat{T} \to -\infty. \tag{105}$$

The formulation (95) already contains the behaviour as $\hat{T} \to -\infty$ with $Y = O(1)$; since we shall also require an exponentially small correction term for $Y = O(-\hat{T})$, we write

$$\mathcal{F}_0 \sim Y/(-\hat{T}) + Y_\infty(\hat{T}) + E$$

and linearise in E to give

$$E_{\hat{T}} = E_{YY} + \frac{3}{(-\hat{T})}E - \left(\frac{Y}{(-\hat{T})} + Y_\infty\right)E_Y. \tag{106}$$

Introducing $\zeta = Y/(-\hat{T})$ and using (105), we have

$$E_{\hat{T}} + \frac{1}{(-\hat{T})}(2\zeta+1)E_\zeta \sim \frac{1}{(-\hat{T})^2}E_{\zeta\zeta} - \frac{1}{(-\hat{T})^2}E_\zeta + \frac{3}{(-\hat{T})}E \qquad \text{as } \hat{T} \to -\infty. \tag{107}$$

In view of the need to match as $\zeta \to 0^-$ into the term $-\mathrm{e}^Y/(-\hat{T})$ in (95), the required expansion for (107) in the limit $\hat{T} \to -\infty$ takes the WKBJ form

$$E \sim \frac{1}{(-\hat{T})}a_0(\zeta)\mathrm{e}^{-(-\hat{T})\phi(\zeta)}, \tag{108}$$

implying

$$\phi - (2\zeta+1)\phi_\zeta = \phi_\zeta^2, \tag{109}$$

in which the right-hand side represents the contribution of viscosity, and

$$a_0 + (2\zeta+1)a_{0\zeta} = -2\phi_\zeta a_{0\zeta} - \phi_{\zeta\zeta}a_0 + \phi_\zeta a_0 + 3a_0, \tag{110}$$

subject to

$$\phi \sim -\zeta, \quad a_0 \to -1 \qquad \text{as } \zeta \to 0^-.$$

Equation (109) can be reduced to autonomous form by writing $\phi = (\zeta+\frac{1}{2})^2\psi(\log|\zeta+\frac{1}{2}|)$, yielding

$$\left(\sqrt{\phi + (\zeta+1/2)^2} + (\zeta+1/2)\right)^2\left(2\sqrt{\phi+(\zeta+1/2)^2} - (\zeta+1/2)\right) = 1/2, \tag{111}$$

from which it follows that

$$\phi \sim \sqrt{\tfrac{2}{3}}(-\zeta)^{1/2} - \tfrac{1}{4}\sqrt{\tfrac{2}{3}}(-\zeta)^{-1/2} + O(1/(-\zeta)) \qquad \text{as } \zeta \to -\infty. \tag{112}$$

Using (109), we obtain the required solution to (110) as

$$a_0 = -\frac{\mathrm{e}^{-\phi_\zeta} - 1}{(-\phi_\zeta)^3(-(2\zeta+1+2\phi_\zeta))^{1/2}}, \tag{113}$$

so that

$$a_0 \sim -\frac{\mathrm{e}^{-1}6^{3/2}}{2^{1/2}}(-\zeta) \qquad \text{as } \zeta \to -\infty. \tag{114}$$

6.3. THE LIMIT $Y \to -\infty$

The way in which the blow-up behaviour of (95) in the limit $\hat{T} \to 0^-$ is selected is somewhat similar to that in which the minimum-speed travelling wave is selected by appropriate initial-value problems for Fisher's equation (an analogy we expand upon in Appendix A.2 by discussing possible similarity solutions to the inviscid RPJ equation). In particular, a crucial step involves determining an exponentially small term in the far-field behaviour of (95).

The relevant balance is again given by (106), but the viscous term is negligible in the limit $Y \to -\infty$ (as is the case in the terms given in (112)), so that

$$E \sim \frac{1}{(-\hat{T})^3}\hat{E}\left((-\hat{T})Y - \int^{\hat{T}} (-T')Y_\infty(T')\,\mathrm{d}T'\right) \tag{115}$$

for some function $\hat{E}(\hat{\omega})$ which cannot be determined for $\hat{\omega} = O(1)$ without solving the full problem but which, by use of (112–114), satisfies

$$\hat{E}(\hat{\omega}) \sim -\frac{\mathrm{e}^{-1}6^{3/2}}{2^{1/2}}(-\hat{\omega})\mathrm{e}^{-\sqrt{2/3}(-\hat{\omega})^{1/2}} \qquad \text{as } \hat{\omega} \to -\infty. \tag{116}$$

6.4. THE LIMIT $\hat{T} \to 0^-$

We are now in a position to address the blow-up behaviour of (95). In the limit $\hat{T} \to 0^-$ we have

$$\mathcal{F}_0 \sim \mathcal{F}_c(Y) \qquad \text{for } Y = O(1) \tag{117}$$

with

$$\mathcal{F}_c(0) = 1, \quad \mathcal{F}_{cY}(0) = 0; \tag{118}$$

$\mathcal{F}_c(Y)$ for $Y > 0$ depends on the evolution over earlier times and cannot be determined without solving the full problem.

For large $-Y$, specifically for $-Y = O(-\log(-\hat{T})/(-\hat{T}))$, the appropriate balance as $\hat{T} \to 0^-$ is of the form

$$\mathcal{F}_0 \sim \frac{-\log(-\hat{T})}{(-\hat{T})^2}\Omega(\xi), \quad \xi = \frac{Y(-\hat{T})}{-\log(-\hat{T})} \tag{119}$$

(see Appendix A.2 for related considerations) with

$$\Omega_\xi - \xi\Omega_{\xi\xi} = \Omega_\xi^2 - \Omega\Omega_{\xi\xi}, \tag{120}$$

the viscous term being negligible, so that

$$\Omega(\xi) = \xi + \xi_0 - \xi_0\mathrm{e}^{\xi/\xi_0} \tag{121}$$

for some constant ξ_0. Matching with (116) as $\xi \to -\infty$ (a procedure which involves the matching of exponentially small terms) implies that $\xi_0 = 3$ with

$$Y_\infty(\hat{T}) \sim \frac{3(-\log(-\hat{T}))}{(-\hat{T})^2} + \frac{3\log(-\log(-\hat{T}))}{(-\hat{T})^2} + \frac{9\log 3}{2(-\hat{T})^2} \qquad \text{as } \hat{T} \to 0^-, \tag{122}$$

indicating the time-dependence of the next two terms required in the expansion (119). It follows from the behaviour of (121) as $\xi \to 0^-$ that in (117) we have

$$\mathcal{F}_c(Y) \sim -\tfrac{1}{6}Y^2/\log(-Y) \qquad \text{as } Y \to -\infty, \tag{123}$$

so on this timescale the interior zero of $\mathcal{F}$ tends to some fixed location $Y = Y_z(\epsilon) = O(1)$, where $\mathcal{F}_c(Y_{z0}) = 0$, this representing its closest approach to the right-hand boundary $y = 1$.

6.5. TURN-AROUND TIME SCALE: $\hat{T} = O(1/\log(1/\epsilon))$

We conclude this section by discussing an intermediate timescale on which (117) ceases to apply (it does not in fact persist for very long) but (97), (99) and (119) remain applicable. On the timescale $T^\ddagger = O(1)$, where

$$\hat{T} = T^\ddagger/\log(1/\epsilon), \tag{124}$$

we have that the pressure coefficient

$$p \sim -\frac{\log(1/\epsilon)}{\epsilon^2(-T^\ddagger)^2};$$

for $Y = O(1)$ we thus have

$$\mathcal{F}_{0YT^\ddagger} = -\frac{1}{(-T^\ddagger)^2}, \qquad \mathcal{F}_0 = \mathcal{F}_c(Y) - Y/(-T^\ddagger) \tag{125}$$

for $T^\ddagger = O(1)$, showing how the interior zero of $\mathcal{F}$ begins to move inwards (further away from $y = 1$) on this time scale. There is also a subsidiary boundary layer with $Y = O(1/\log^{1/2}(1/\epsilon))$, which is required to satisfy the condition $\mathcal{F}_y = 0$ on $y = 1$.

7. Time-dependent flows: asymptotics of the fastest phases

7.1. $\hat{T} = O(\epsilon \log^2(1/\epsilon))$

7.1.1. *Preamble*

This is the timescale on which it follows from (119) that the boundary layer (95) merges with the intermediate region described by (96–97). We write

$$\hat{T} = \epsilon \log^2(1/\epsilon)\hat{\tau}, \qquad \mathcal{F} = H/\epsilon^2 \log^3(1/\epsilon), \tag{126}$$

so (119) implies the matching condition

$$H_0 \sim \frac{1}{(-\hat{\tau})^2}\Omega(\xi), \qquad \xi = \hat{Y}(-\hat{\tau}) \tag{127}$$

as $\hat{\tau} \to -\infty$ with $\hat{Y} = O(1/(-\hat{\tau}))$, where

$$\Omega(\xi) = \xi + 3 - 3\mathrm{e}^{\xi/3}. \tag{128}$$

Away from $y = 1$, the analysis of Section 5.1.4 is still pertinent on earlier timescales, so (76) implies the matching condition

$$H_0 \sim -\frac{1}{(-\hat{\tau})}\left(1 - \mathrm{e}^{\hat{Y}}\right) \tag{129}$$

as $\hat{\tau} \to -\infty$ with $\hat{Y} = O(1)$.

We have for $\hat{Y} = O(1)$ the inviscid balance that

$$H_{0\hat{Y}\hat{\tau}} = H_{0\hat{Y}}^2 - H_0 H_{0\hat{Y}\hat{Y}}. \tag{130}$$

In view of (125) the boundary conditions on (130) are

$$\left.\begin{array}{ll} \text{as } \hat{Y} \to 0^- & H_0 \sim -\frac{1}{6}\hat{Y}^2, \\ \text{as } \hat{Y} \to -\infty & H_{0\hat{Y}} \to 0, \end{array}\right\} \tag{131}$$

where we have matched as $\hat{Y} \to -\infty$. We now present the solution to (130) subject to (127), (129) and (131).

7.1.2. *Boundary layer solution*

The approach outlined in Appendix A.1 can be used to derive the required solution. Omitting the details of the derivation, we find the solution in terms of a parameter ζ_i (which parametrises the characteristics of (130)) in the form

$$\hat{Y} = -\int_{\zeta_i}^{\infty} \frac{\mathrm{d}\zeta}{\mathrm{e}^{\zeta/3} - \zeta - \hat{\tau}}, \qquad H_0 = -\int_{\zeta_i}^{\infty} \frac{\mathrm{d}\zeta}{(\mathrm{e}^{\zeta/3} - \zeta - \hat{\tau})^2}. \tag{132}$$

The crucial characteristics have

$$\hat{Y}(-\hat{\tau}) = -3\log(-\hat{\tau}) + O(1) \qquad \text{as } \hat{\tau} \to -\infty, \tag{133}$$

and thus lie in the overlap regime between (127) and (129); (132) is thus best derived from a composite (uniformly valid) representation such as

$$H_0 \sim \frac{3}{(-\hat{\tau})^2}\left(1 - \mathrm{e}^{(-\hat{\tau})\hat{Y}/3}\right) - \frac{1}{(-\hat{\tau})}\left(1 - \mathrm{e}^{\hat{Y}}\right) \qquad \text{as } \hat{\tau} \to -\infty. \tag{134}$$

In addition to (132), we have

$$H_{0\hat{Y}} = \frac{1}{\mathrm{e}^{\zeta_i/3} - \zeta_i - \hat{\tau}}, \qquad H_{0\hat{Y}\hat{Y}} = -\frac{\frac{1}{3}\mathrm{e}^{\zeta_i/3} - 1}{\mathrm{e}^{\zeta_i/3} - \zeta_i - \hat{\tau}}, \tag{135}$$

so that

$$H_{0\hat{Y}\hat{Y}} = 0 \qquad \text{on the characteristic } \zeta_i = 3\log 3. \tag{136}$$

For matching purposes we need the following consequences of (132). Firstly,

$$H_0 \sim -\int_{-\infty}^{\infty} \frac{\mathrm{d}\zeta}{(\mathrm{e}^{\zeta/3} - \zeta - \hat{\tau})^2} \qquad \text{as } \hat{Y} \to -\infty. \tag{137}$$

Secondly, H_0 blows up as $\hat{\tau} \to \hat{\tau}_c^-$, where

$$\hat{\tau}_c = -3(\log 3 - 1). \tag{138}$$

It then follows, if we use (132) along the characteristics with $\zeta_i = 3\log 3 + O((\hat{\tau}_c - \hat{\tau})^{1/2})$ (*cf.* (136)), that

$$H_0 \sim \frac{\hat{Y}}{2(\hat{\tau}_c - \hat{\tau})} - \frac{3^{1/2}}{2^{3/2}(\hat{\tau}_c - \hat{\tau})^{3/2}} \sin\left(\frac{2^{1/2}(\hat{\tau}_c - \hat{\tau})^{1/2}\hat{Y}}{3^{1/2}}\right), \tag{139}$$

for $\hat{Y} = O((\hat{\tau}_c - \hat{\tau})^{-1/2})$ with $-6^{1/2}\pi < \hat{Y}(\hat{\tau}_c - \hat{\tau})^{1/2} < 0$, and

$$H_0 \sim -\frac{3^{1/2}\pi}{2^{1/2}(\hat{\tau}_c - \hat{\tau})^{3/2}} \tag{140}$$

for $\hat{Y} = O((\hat{\tau}_c - \hat{\tau})^{-1/2})$ with $\hat{Y}(\hat{\tau}_c - \hat{\tau})^{1/2} < -6^{1/2}\pi$, consistent with (137). Appendix A.2 clarifies why (139–140) is the self-similar form appropriate for describing the current intermediate asymptotic behaviour.

As $\hat{\tau} \to \hat{\tau}_c^-$ with $\hat{Y} = O(1)$ we have that

$$H_0 \sim H_c(\hat{Y}), \tag{141}$$

where H_c is given by

$$\hat{Y} = -\int_{\zeta_i}^{\infty} \frac{\mathrm{d}\zeta}{\mathrm{e}^{\zeta/3} - \zeta + 3(\log 3 - 1)}, \qquad H_c = -\int_{\zeta_i}^{\infty} \frac{\mathrm{d}\zeta}{(\mathrm{e}^{\zeta/3} - \zeta + 3(\log 3 - 1))^2}, \tag{142}$$

so that

$$H_c \sim -\tfrac{1}{6}\hat{Y}^2 \quad \text{as } \hat{Y} \to 0^-, \qquad H_c \sim \tfrac{1}{18}\hat{Y}^3 \quad \text{as } \hat{Y} \to -\infty, \tag{143}$$

consistent with (131) and matching with (139). Finally, there is a similar region with

$$\hat{Y} = \hat{Y}_c(\hat{\tau}) + O(1), \qquad \text{where } \hat{Y}_c \sim -6^{1/2}\pi(\hat{\tau}_c - \hat{\tau})^{-1/2},$$

which provides a smooth transition between (139) and (140); we omit details, however.

7.1.3. *Other regions*

For $y = O(1)$ we have (*cf.* (98–99)), writing $H \sim \hat{H}_0(y, \hat{\tau})$, that

$$\hat{H}_{0y y\hat{\tau}} = 0$$

so that

$$\hat{H}_0 = -\frac{1}{2}\int_{-\infty}^{\infty} \frac{\mathrm{d}\zeta}{(\mathrm{e}^{\zeta/3} - \zeta - \hat{\tau})^2}(y + 1), \tag{144}$$

where we have matched with (137). This implies that

$$\hat{H}_0 \sim -\frac{3^{1/2}\pi}{2^{3/2}(\hat{\tau}_c - \hat{\tau})^{3/2}}(y + 1) \qquad \text{as } \hat{\tau} \to \hat{\tau}_c^-. \tag{145}$$

Lastly, the analogous region to that described by (100) has

$$y = -1 + \epsilon^{3/2}\log(1/\epsilon)\tilde{y}, \qquad \mathcal{F} = \tilde{\mathcal{H}}/\epsilon^{1/2}\log^2(1/\epsilon) \tag{146}$$

with, by use of (101),

$$\left.\begin{array}{ll} & \tilde{\mathcal{H}}_{0\tilde{y}\tilde{y}\hat{\tau}} = \tilde{\mathcal{H}}_{0\tilde{y}\tilde{y}\tilde{y}\tilde{y}}, \\ \text{at } \tilde{y} = 0 & \tilde{\mathcal{H}}_0 = \tilde{\mathcal{H}}_{0\tilde{y}} = 0, \\ \text{as } \tilde{y} \to +\infty & \tilde{\mathcal{H}}_0 \sim -\frac{1}{2}\displaystyle\int_{-\infty}^{\infty} \frac{\mathrm{d}\zeta}{(\mathrm{e}^{\zeta/3} - \zeta - \hat{\tau})^2}\tilde{y}, \\ \text{as } \hat{\tau} \to -\infty & \tilde{\mathcal{H}}_0 \sim \dfrac{1}{2(-\hat{\tau})^{1/2}}\Phi\left(\tilde{y}/(-\hat{\tau})^{1/2}\right), \end{array}\right\} \tag{147}$$

where $\Phi(\eta)$ is given by (102) (we note that, as with (100), the nonlinear terms in (1) are of relative size $O(1/\log(1/\epsilon))$ here, so are only just negligible in (147)). In view of (145) we have blow-up behaviour of the form

$$\tilde{\mathcal{H}}_0 \sim \frac{1}{(\hat{\tau}_c - \hat{\tau})}\Psi\left(\frac{\tilde{y}}{(\hat{\tau}_c - \hat{\tau})^{1/2}}\right) \qquad \text{as } \hat{\tau} \to \hat{\tau}_c^-, \tag{148}$$

where

$$\Psi(\eta) = -\frac{3^{1/2}\pi}{2^{3/2}}\eta(1 - \mathrm{e}^{\eta^2/4}\,\mathrm{erfc}\,(\tfrac{1}{2}\eta)). \tag{149}$$

7.2. $\hat{\tau} = \hat{\tau}_c + O(1/\log^2(1/\epsilon))$

We now discuss the final, and fastest, phase of evolution, in which the interior zero moves rapidly from the neighbourhood of $y = 1$ to that of $y = 0$. We write

$$\hat{\tau} = \hat{\tau}_c + \bar{\tau}/\log^2(1/\epsilon), \qquad \mathcal{F} = \mathcal{H}/\epsilon^2, \tag{150}$$

this being (in view of (139–140)) the timescale on which the boundary layer of Section 7.1.2 merges with the outer region. At leading order we have in the outer region $y = O(1)$ that

$$\mathcal{H}_{0yy\bar{\tau}} = \mathcal{H}_{0y}\mathcal{H}_{0yy} - \mathcal{H}_0\mathcal{H}_{0yyy}, \tag{151}$$

i.e. an inviscid balance but, in contrast to (130), one in which a non-zero pressure coefficient $\mathcal{P}_0(\bar{\tau})$ is to be determined as part of the solution to (151), with

$$p \sim \mathcal{P}_0(\bar{\tau})/\epsilon^4, \qquad \mathcal{H}_{0y\bar{\tau}} = \mathcal{H}_{0y}^2 - \mathcal{H}_0\mathcal{H}_{0yy} + \mathcal{P}_0(\bar{\tau}). \tag{152}$$

From (145) we have

$$\mathcal{H}_0 \sim -\frac{3^{1/2}\pi}{2^{3/2}(-\bar{\tau})^{3/2}}(y+1) \qquad \text{as } \bar{\tau} \to -\infty \text{ with } y = O(1) \tag{153}$$

and, since $\mathcal{H}_{0yy} = 0$ holds for all time along characteristics of (151) if it does so initially, we are motivated to seek a solution of the form

$$\left.\begin{array}{ll} \mathcal{H}_0 = -\mathcal{A}(\bar{\tau})(1-y) + \mathcal{B}(\bar{\tau})\sin(\bar{\lambda}(\bar{\tau})(1-y)) & y > \mathcal{S}(\bar{\tau}), \\ \mathcal{H}_0 = -\mathcal{E}(\bar{\tau})(y+1) & y < \mathcal{S}(\bar{\tau}), \end{array}\right\} \tag{154}$$

for some $\mathcal{S}(\bar{\tau})$ which is to be determined as part of the solution. The admissibility of such a 'two part' solution stems from the hyperbolic character of (151) and from matching with (139–140), which imply that

$$\left.\begin{array}{ll} \mathcal{S}(\bar{\tau}) \sim 1 - 6^{1/2}\pi/(-\bar{\tau})^{1/2} & \text{as } \bar{\tau} \to -\infty \\ \mathcal{H}_0 \sim -\dfrac{(1-y)}{2(-\bar{\tau})} + \dfrac{3^{1/2}}{2^{3/2}(-\bar{\tau})^{3/2}}\sin\left(\dfrac{2^{1/2}(-\bar{\tau})^{1/2}}{3^{1/2}}(1-y)\right) & \text{as } \bar{\tau} \to -\infty,\ y > \mathcal{S}(\bar{\tau}); \end{array}\right\} \tag{155}$$

in writing down (154) we have used the fact that $\mathcal{H}_{0yy} = 0$ on $y = 1$ as well as in $y < \mathcal{S}(\bar{\tau})$, the characteristic projections of (151) satisfying

$$\frac{\mathrm{d}y}{\mathrm{d}\bar{\tau}} = \mathcal{H}_0,$$

so that $y = 1$ is a characteristic, as is $y = \mathcal{S}(\bar{\tau})$. The analyticity of the solution is maintained via an interior layer about $\mathcal{S}(\bar{\tau})$ (*cf.* the discussion of Appendix A.2). The continuity conditions on (154) are

$$\text{at } y = \mathcal{S}(\bar{\tau}) \qquad [\mathcal{H}_0]^+_- = [\mathcal{H}_{0y}]^+_- = [\mathcal{H}_{0yy}]^+_- = 0,$$

and from these and (151) it is straightforward to deduce that, up to translations in $\bar{\tau}$,

$$\left.\begin{aligned} &\tfrac{1}{2}\bar{\lambda}^2 + \pi\bar{\lambda} + \pi^2 \log(\bar{\lambda} - \pi) = \tfrac{1}{3}(-\bar{\tau}), \\ &\mathcal{S} = 1 - \frac{2\pi}{\bar{\lambda}}, \quad \mathcal{A} = \frac{\bar{\lambda} - \pi}{3\bar{\lambda}^3}, \quad \mathcal{B} = \frac{1}{3\bar{\lambda}^3}, \quad \mathcal{E} = \frac{\pi}{3\bar{\lambda}^3}. \end{aligned}\right\} \tag{156}$$

It follows that as $\bar{\tau} \to +\infty$

$$\bar{\lambda} \to \pi^+, \qquad \mathcal{S} \to (-1)^+, \tag{157}$$

at an exponentially fast rate, with

$$\mathcal{H}_0 \sim \frac{1}{3\pi^3} \sin(\pi y) \qquad \text{for } y > \mathcal{S}(\bar{\tau}), \tag{158}$$

which brings us full circle back to (46), confirming that the *ansatz* (39) is appropriate and identifying the final unknown as

$$C_I(\epsilon) \sim \frac{1}{3\pi^3\epsilon^2}, \tag{159}$$

and completing the analysis of the limit cycle behaviour. Both $\mathcal{F}$ and $-p$ attain their maximum values as $\bar{\tau} \to +\infty$ (*cf.* Figure 10), with

$$p \sim -\frac{1}{9\pi^4\epsilon^2}.$$

Viscous effects now come back into play, with the solution decaying slowly due to viscous dissipation, as described by (47–48).

The final loose ends concern the behaviour in the boundary layers on this timescale; the relevant scalings are $y = \pm 1 + O(\epsilon^{3/2})$ and $\mathcal{F} = O(\epsilon^{-1/2})$, and the full balance occurs at leading order in both the boundary layers (in view of (157), the range $y < \mathcal{S}(\bar{\tau})$ merges into the left-hand boundary layer for sufficiently large $\bar{\tau}$). In the right-hand boundary layer, there is again an intermediate timescale, analogous to that discussed in Section 6.5, on which (141) ceases to hold. Since

$$\mathcal{P}_0 = -\frac{\pi}{3\bar{\lambda}^5} + \frac{2\pi^2}{9\bar{\lambda}^6}, \tag{160}$$

we have

$$\mathcal{P}_0 \sim \frac{3^{3/2}\pi}{2^{5/2}(-\bar{\tau})^{5/2}} \qquad \text{as } \bar{\tau} \to -\infty$$

and the relevant timescale is

$$\bar{\tau} = \log^{4/3}(1/\epsilon)\tau^{\ddagger}$$

with

$$H_{0\hat{Y}\tau^{\ddagger}} = -\frac{3^{3/2}\pi}{2^{5/2}(-\tau^{\ddagger})^{5/2}}, \qquad H_0 = H_c(\hat{Y}) - \frac{3^{1/2}\pi\hat{Y}}{2^{3/2}(-\tau^{\ddagger})^{3/2}}. \tag{161}$$

A noteworthy reinterpretation of (154) involves consideration of the quantity

$$\Pi(y,t) = \mathcal{F}_{yyy}^2 - \mathcal{F}_{yy}\mathcal{F}_{yyyy}.$$

For $\epsilon = 0$ it follows from (1) that

$$\Pi_t = -\mathcal{F}\Pi_y \tag{162}$$

so that Π is constant along characteristics; moreover, for any ϵ, for which

$$\Pi_t + \mathcal{F}\Pi_y = \epsilon\left(\frac{2}{\mathcal{F}_{yy}}\left(\mathcal{F}_{yyyy}\Pi - \mathcal{F}_{yyy}\Pi_y\right) + \Pi_{yy}\right), \tag{163}$$

the *ansatz* (39) corresponds exactly to Π ($= \lambda^6(C^2 + D^2)$) being independent of y, whereby $\mathcal{F}_{yyyy} = -\lambda^2\mathcal{F}_{yy}$ and (163) reduces to (42). The solution (154) has Π piecewise constant (a feature first established by the intermediate asymptotic similarity solution (139–140)), with its value in $y < \mathcal{Y}(\bar{\tau})$ (zero for the leading-order solution $\mathcal{H}_0$) being the remnant after viscous dissipation (*cf.* (42)) of the previous oscillation. This 'old' value is swept out by a 'new' one (the one which holds in $y > \mathcal{Y}(\bar{\tau})$) whose value is that required to obtain periodic behaviour by decaying to the 'old' value in the course of the oscillation. With this interpretation, the leading-order value of Π ($\sim 1/9\epsilon^4$) can be deduced (given (162)) from the second of (143), without any need to solve (151). Indeed, the details of the analysis of Section 7.1 can also be circumvented – the solutions (127) and (129) each correspond to $\Pi = 0$, so the characteristics on which Π is non-zero emanate from the overlap region (133); the blow-up behaviour is dominated by the characteristic on which $H_{0\hat{Y}\hat{Y}} = 0$, so that $H_{0\hat{Y}}$ is maximal, and this satisfies

$$\hat{Y} \sim \frac{3}{(-\hat{\tau})}\log(3(-\hat{\tau})) \qquad \text{as } \hat{\tau} \to -\infty$$

and has, by use of (134), $\Pi \sim 1/9\epsilon^4$. Since the blow-up behaviour (139–140) dictates the subsequent evolution, this determines the 'new' value of Π; the calculation just given emphasises the importance of the composite expression of (134) in describing the overlap between the ranges of validity of (127) and (129), as well as the crucial role played by the timescale of Section 6, since this can be viewed as being responsible for the 'new' value. Plotting Π from the numerical solutions of Section 4 provides (given the relatively large values of ϵ in the simulations) strong support for the scenario described above.

8. Discussion

The asymptotic analysis of the time-dependent problem outlined above leads to a remarkable degree of analytical progress, involving a variety of nonlinear techniques. The key aspects of the evolution are described by the low-dimensional reduction of Section 5 and by the $\alpha = 1$ and $\alpha = 1/2$ similarity solutions of Appendix A.2 (which can be viewed as similarity solutions of the second kind, *cf.* [27], albeit selected in a rather delicate way); in addition the determination of the values of the constants in (121) and (139), corresponding to λ_0 in

each of (A12) and (A13), requires respectively the matching of exponentially small terms and the solution of (130) by characteristic methods. Detailed comparison between numerical and asymptotic results is not currently possible, largely because the numerical approach cannot be applied with ϵ small enough for a convincing comparison, particularly given the prevalence of terms in $\log(1/\epsilon)$ in many of the expansions; nevertheless, a comparison based on crude extrapolation to $\epsilon \to 0$ of quantities obtained numerically for a variety of ϵ yields encouraging results. Moreover, the asymptotic results successfully capture all the qualitative features of the numerics (*cf.* Figure 5 in particular), as well as the orders of magnitude of the various quantities. Thus the asymptotic approach is currently the only way to construct the limit cycles for very small ϵ and is very valuable in clarifying how the evolution proceeds and why numerical approaches encounter difficulties when ϵ is small (in particular, the period of the oscillation scales as $t = O(\log(1/\epsilon)/\epsilon)$ (see (50); $(\log(C_I(\epsilon))/\pi^2 + T_{c0})/\epsilon$ provides an estimate of the period), while on the fastest phase (see (150)) t varies by an $O(\epsilon^2)$ amount). While the analysis is sufficiently complicated that the validity of all the algebraic details cannot of course be guaranteed, the approach of Appendix A.2 provides independent verification of the key role played by the $\alpha = 1$ and $\alpha = 1/2$ similarity solutions; the values of λ_0 in (A12) and (A13) cannot be determined solely by such an approach, though, so these two constants are likely to be the quantities most susceptible to error.

The inviscid version of the RPJ equation

$$\mathcal{F}_{0yyt} = \mathcal{F}_{0y}\mathcal{F}_{0yy} - \mathcal{F}_0\mathcal{F}_{0yyy}, \qquad \mathcal{F}_{0yt} = \mathcal{F}_{0y}^2 - \mathcal{F}_0\mathcal{F}_{0yy} + p_0(t)$$

plays a central role in our analysis and has characteristic projections

$$\frac{\mathrm{d}y}{\mathrm{d}t} = \mathcal{F}_0(y,t) \tag{164}$$

on which

$$\frac{\mathrm{d}\mathcal{F}_{0y}}{\mathrm{d}t} = \mathcal{F}_{0y}^2 + p_0(t), \qquad \frac{\mathrm{d}\mathcal{F}_{0yy}}{\mathrm{d}t} = \mathcal{F}_{0y}\mathcal{F}_{0yy} \tag{165}$$

(*cf.* Appendix A.1; the Lagrangian equation for x corresponding to (164) is

$$\frac{\mathrm{d}x}{\mathrm{d}t} = -x\mathcal{F}_{0y}(y,t),$$

it being noteworthy that this furnishes the linearising transformation for the Riccati equation given by the first of (165). Moreover, from (4) we have

$$\frac{\mathrm{d}\mathcal{F}_0}{\mathrm{d}t} = -\hat{p}_y, \qquad \frac{\mathrm{d}}{\mathrm{d}t}(x\mathcal{F}_{0yy}) = 0,$$

the second of which corresponds to vorticity conservation along characteristics). An issue alluded to above concerns the fact that it follows from (164) that the characteristics near $y = 1$ leave the fluid domain (since $\mathcal{F}_0(1,t) = 1$), whereas information needs to be fed back into the fluid for the solution to remain bounded and for the limit cycle to turn around. This is accomplished in two ways. During the later stages of turn-around one has $\mathcal{F} \gg 1$ so that (as in (131)) the leading-order inviscid problem sees zero normal velocity at the wall and there is within the leading-order formulation (*cf.* (127), (129)) an infinite amount of time for the

information to propagate in. More noteworthy, however, are the earlier stages of this process; if we write

$$\mathcal{F} \sim \sum_{n=0}^{\mathcal{N}} \mu_n(\epsilon)\mathcal{F}_n(y,t) + \nu_0(\epsilon)\Psi_0(y,t)\mathrm{e}^{-\Phi(y,t)/\epsilon} \qquad \text{as } \epsilon \to 0,$$

where $\mu_0(\epsilon) = 1$ and the summation gives the algebraic expansion for $\mathcal{F}$, with $\mathcal{N}(\epsilon)$ being its optimal truncation point (such a procedure enables the exponentially small term to be legitimately separated off in very general contexts, *cf.* [28]), then (away from Stokes lines, of which we avoid discussion here) we have from (1) that

$$\Phi_t = -\Phi_y^2 - \mathcal{F}_0\Phi_y. \tag{166}$$

Equation (166) has characteristic projections

$$\frac{\mathrm{d}y}{\mathrm{d}t} = \mathcal{F}_0(y,t) + 2\Phi_y(y,t), \tag{167}$$

the final term of which represents the effects of viscosity; since the constraints $\Phi(1,t) = 0$, $\Phi_y(1,t) = -1$ are required in order to match into the viscous boundary layer, (167) implies that information does indeed propagate back into the fluid, a feature which underpins the matching of exponentially small terms in Section 6.

The reduction (39), (68) is noteworthy for a number of reasons. Firstly, it provides a large family of exact solutions to the incompressible Navier–Stokes equations, for which some generalisations are available – for example, via solutions of the form $\psi = \Psi(y,t) - x\mathcal{F}(y,t)$, $p = \hat{p}(y,t) + xP(t) + x^2p(t)/2$ satisfying (3), (4) and

$$\Psi_{yt} = \epsilon\Psi_{yyy} + \Psi_y\mathcal{F}_y - \mathcal{F}\Psi_{yy} - P(t);$$

of course, in the Navier–Stokes (rather than RPJ) context there are important issues concerning the stability or otherwise of the solutions we have described. Secondly, it plays a very valuable (and concise) role in providing a uniformly valid description of the outer behaviour over each of the timescales discussed in Section 5.1; we stress that this reduction is valid in the current context only in the asymptotic limit $\epsilon \to 0$, for which it provides an immense saving in computational time. The concept of a uniformly valid expansion is very well-established (see, for example, [29]), but such examples motivate us to comment on 'uniformly valid equations', whereby the original formulation is replaced by a simpler one which has the same asymptotic behaviour; the resulting simplified formulation may be very convenient for numerical (as well as asymptotic) studies, particularly when the stiffness of the original problem can be removed in this fashion. The concept can be illustrated by giving a reinterpretation of an example discussed in Appendix 1 of [30], namely

$$u_t = \left((u+\epsilon)^m u_x\right)_x \tag{168}$$

with $0 < \epsilon \ll 1$, $m > 0$. For $\epsilon = 0$, Equation (168) has compactly supported solutions and an analysis of the limit $\epsilon \to 0$ clarifies how this property is lost for positive ϵ; a very concise presentation of such a limit (which is guided by the asymptotics) introduces the quantity

$$v = \int_0^u \left(\frac{(u'+\epsilon)^m}{u'} - \frac{\epsilon^m}{u'}\right) \mathrm{d}u' + \epsilon^m \log u, \tag{169}$$

giving the uniformly valid leading-order equation

$$v_{0t} = m v_0 H(v_0) v_{0xx} + v_{0x}^2, \tag{170}$$

where H is the Heaviside step function. Equation (170) encompasses each of the three regions appearing in [30] in a single equation and makes explicit the hyperbolic character of the low concentration tail. Moreover, the simplification to (170) permits a family of similarity solutions, notably

$$v_0 = t^{-m/(m+2)} V(x/t^{1/(m+2)}), \tag{171}$$

not shared by the full equation (168); (171) provides a uniformly valid expression of the asymptotic behaviour for δ-function initial data for u. It is worth noting that, because the nonlinearity in (170) is not analytic in v_0, care is needed when applying classical Lie group techniques to identify such similarity reductions.

We conclude by drawing together the analyses of the steady-state and time-dependent problems by outlining for small ϵ the role played in the transient problem by the unstable equilibrium solution. It is noteworthy that the outer steady-state solution (29) is of the form (39), but the relationship between the two problems is somewhat subtle, with no region completely analogous to the interior layer of Section 3.4.2 featuring in the time-dependent analysis. When the steady-state solution is perturbed, time-dependent effects make their first appearance in the $O(\nu^2)$ term of (23), thereby introducing a time derivative into (28); a number of timescales are needed to describe this, each having $\epsilon t = O(\log^q(1/\epsilon))$ for some q. The conclusion regarding the behaviour subsequent to these timescales is that if the steady state is (roughly speaking) perturbed by moving the interior zero towards $y = 0$, then the solution quickly locks onto the (slow) viscous-dominated phase of evolution (51–52), the instability of the steady state corresponding to the instability from above of the fixed point $\lambda_0 = \pi/2$ of (52), from which λ_0 then increases to λ_c (leading onto the faster phases). Conversely, if the interior zero is perturbed towards $y = 1$, the solution instead enters the (fast) inviscid phase, given by (63) with the $\frac{1}{2}$'s negligible because $D_0 \gg 1$. In view of (29), (31), the relevant scalings are

$$\hat{t} = \epsilon \log(1/\epsilon) t^{\ddagger}, \qquad D_0 = D_0^{\ddagger}/\epsilon \log(1/\epsilon), \qquad C_0 = C_0^{\ddagger}/\epsilon \log(1/\epsilon),$$

with

$$D_0^{\ddagger} \to -\frac{1}{4\pi}, \qquad C_0^{\ddagger} \to 0, \qquad \lambda_0 \to (\pi/2)^- \qquad \text{as } t^{\ddagger} \to -\infty,$$

from which it follows that

$$D_0^{\ddagger} = -\frac{1}{4\pi}\left(\frac{\pi}{2\lambda_0}\right)^3 \sin\lambda_0, \qquad C_0^{\ddagger} = -\frac{1}{4\pi}\left(\frac{\pi}{2\lambda_0}\right)^3 \cos\lambda_0,$$

and

$$\frac{\mathrm{d}\lambda_0}{\mathrm{d}t^{\ddagger}} = -\frac{1}{8\pi}\left(\frac{\pi}{2}\right)^3 \frac{\sin 2\lambda_0}{\lambda_0^2}, \tag{172}$$

the instability of the steady state corresponding to (172) also having an unstable fixed point at $\lambda_0 = \pi/2$. The solution to (172) then drops to zero (*cf.* (66)), leading onto behaviour comparable to that described above. The unstable steady state can thus be viewed as providing a borderline between initial conditions which evolve onto the slow part of the limit cycle (with

y_z initially decreasing) and those which lead rapidly into the fast phases (with y_z, already close to $y = 1$ for the steady state, initially increasing).

Our ordinary differential equation results of Section 3 are of sufficient accuracy to provide viable representations of the steady-state behaviour for large R, while the partial differential equation results of Sections 4–7 are of practical value in describing the evolution of the RPJ equation in that no straightforward and suitable numerical approach is available for even quite moderately large R; the extent of analytical progress that is possible here makes the asymptotic approach particularly worthwhile. Furthermore, as with many asymptotic studies, valuable insight is provided into the dominant physical balances which occur.

9. Concluding remarks

We hope that the detailed analysis of (1) described above is of interest both from the point of view of asymptotic methods and in view of its relevance as a paradigm problem for the time-dependent Navier–Stokes equations. The variety of asymptotic approaches needed is highlighted at the beginning of Section 8 and the analysis illustrates some of the complexities which arise in studying the asymptotics of time-dependent, spatially heterogeneous solutions to partial differential equations, specifically those exhibiting time dependence in the form of relaxation oscillations.

In the symmetrical version of (1–2), with equal fluid suction velocities at each channel wall, temporally chaotic solutions are found in numerical simulations at moderate Reynolds number [9, 15]. These solutions are analogous to chaotic solutions to the Lorenz system of three ordinary differential equations: the velocity profile may 'flip' about the centre-line $y = 0$ of the channel in an apparently random fashion, just as solutions to the Lorenz system flip between the two wings of the Lorenz attractor. Whether the approaches outlined above would prove equally efficacious in analysing such chaotic behaviour is an intriguing open question. A less speculative extension of our analysis would be in describing the large-amplitude limit-cycle solutions that we have also found in numerical simulations of the symmetrical problem at large Reynolds number, which appear to have a structure close to that of the large-amplitude limit-cycle solutions to the asymmetrical problem given above.

While the asymptotic methods we have used are for the most part well-established, novel features of the current work include the manner in which some of them are applied and the use in combination of such a range; we expect that a similar synthesis of different techniques will prove valuable in many other evolutionary problems. With regard to our steady-state analysis, we would highlight the key role of optimal truncation in making an expansion in inverse powers of the logarithm of the small parameter sufficiently accurate to be useful in practice.

The RPJ equation can play an instructive role as an exact reduction of the Navier–Stokes equations in, for example, studying blow-up phenomena and transitions to chaos. We accordingly hope that some of the apparatus we have developed will also prove useful in the study of the full Navier–Stokes equations or of other similarity reductions thereof. An example of the latter is the flow between a porous rotating disk and an impermeable, fixed plane [31], where a Hopf bifurcation is known to give rise to stable oscillatory solutions, although the time-dependent flow at large Reynolds number remains to be investigated. The natural extension of the RPJ equation to fully three-dimensional flows is also known to exhibit chaotic solutions [32]; these too may be amenable to our approach.

We have given perhaps one of the most detailed asymptotic studies so far undertaken of fully time-dependent nonlinear behaviour in a large Reynolds number flow problem of this type and, as indicated above, we hope that the asymptotic analysis described will be of value in the treatment of a range of related initial–boundary-value problems. Moreover, the current analysis is more broadly of some interest from the point of view of nonlinear parabolic systems, it being rare for scalar parabolic equations to possess temporally periodic ω-limit sets. We hope that the approaches we have outlined will also prove effective in asymptotic studies of a variety of other evolutionary problems arising in a range of contexts.

Acknowledgements

JRK gratefully acknowledges the support of the Leverhulme Trust.

Appendix A. The zero-pressure inviscid Riabouchinsky–Proudman–Johnson equation

A.1. General solution

This appendix is concerned with the partial differential equation

$$\mathcal{F}_{yt} = \mathcal{F}_y^2 - \mathcal{F}\mathcal{F}_{yy}; \tag{A1}$$

this is known to be integrable (*cf.* [15] and references therein) but it is useful in the current context to outline a convenient means by which initial-value problems can be solved for arbitrary initial data. We note that results equivalent to some of those below have also been obtained (in a slightly different context) by Galaktionov and Vazquez [33]; a special case of (39), namely

$$\mathcal{F} = B(t)y + C(t)\sin\lambda(t)y \qquad \text{with } p(t) = 0$$

can be used to exemplify the generic blow-up behaviour they describe. The analysis we give fairly readily generalises to the equation

$$\mathcal{F}_{yt} = \mathcal{F}_y^2 - \mathcal{F}\mathcal{F}_{yy} + p(t)$$

for prescribed $p(t)$ (again see [15]), but in practice the pressure coefficient is typically unknown and we shall not pursue the case $p \not\equiv 0$.

From (A1) we have

$$\mathcal{F}_{yyt} = \mathcal{F}_y\mathcal{F}_{yy} - \mathcal{F}\mathcal{F}_{yyy}, \tag{A2}$$

and so (A1–A2) can be solved by characteristic methods by satisfying

$$\frac{\mathrm{d}y}{\mathrm{d}t} = \mathcal{F}, \tag{A3}$$

$$\frac{\mathrm{d}\mathcal{F}_y}{\mathrm{d}t} = \mathcal{F}_y^2, \qquad \frac{\mathrm{d}\mathcal{F}_{yy}}{\mathrm{d}t} = \mathcal{F}_y\mathcal{F}_{yy} \tag{A4}$$

along the characteristics ((A3) shows that these represent particle paths); given $\mathcal{F}_y \geq 0$, characteristics on which $\mathcal{F}_y$ does not blow up therefore have $\mathcal{F}_y \equiv 0$. For the initial-value problem

$$\text{at } t = 0 \qquad \mathcal{F} = \mathcal{F}_i(y),$$

we impose on each characteristic that

$$\text{at } t = 0 \qquad y = y_i, \qquad \mathcal{F}_y = \mathcal{F}_i'(y_i), \qquad \mathcal{F}_{yy} = \mathcal{F}_i''(y_i),$$

using y_i to parametrise the initial data, and (A4) then gives

$$\mathcal{F}_y = \frac{\mathcal{F}_i'(y_i)}{1 - t\mathcal{F}_i'(y_i)}, \qquad \mathcal{F}_{yy} = \frac{\mathcal{F}_i''(y_i)}{1 - t\mathcal{F}_i'(y_i)}; \tag{A5}$$

moreover, if we write $y = y(t; y_i)$, it follows from (A3) that along characteristics

$$\frac{\mathrm{d}}{\mathrm{d}t}\left(\frac{\partial y}{\partial y_i}\right) = \frac{\partial y}{\partial y_i}\mathcal{F}_y$$

so that

$$\frac{\partial y}{\partial y_i} = \frac{1}{1 - t\mathcal{F}_i'(y_i)}$$

and hence

$$y = \int_0^{y_i} \frac{1}{1 - t\mathcal{F}_i'(\xi)}\,\mathrm{d}\xi + y_a(t), \qquad \mathcal{F} = \int_0^{y_i} \frac{\mathcal{F}_i'(\xi)}{(1 - t\mathcal{F}_i'(\xi))^2}\,\mathrm{d}\xi + \dot{y}_a(t), \tag{A6}$$

where y_a is arbitrary except that $y_a(0) = 0$, $\dot{y}_a(0) = -\mathcal{F}_i(0)$. Expressions (A5) and (A6) furnish the general solution to (A1) in terms of the parameter y_i, as is readily confirmed by direct substitution. Imposing the boundary data

$$y = 0 \qquad \mathcal{F} = \mathcal{F}_y = 0,$$

for example (this being relevant to the analysis of Section 7.1), with $\mathcal{F}_i(0) = \mathcal{F}_i'(0) = 0$, implies that $y_a(0) = 0$. In that context, however, we have the difficulty of wishing to impose initial data as $t \to -\infty$ rather than at $t = 0$, with $y \to 0^+$ as $t \to -\infty$ on characteristics; nevertheless, the initial–boundary-value problem in question can similarly be solved to give (132).

A.2. Similarity solutions

Of particular interest in the preceding analysis are the scaling similarity solutions of (A1), namely

$$\mathcal{F} = (-t)^{-(\alpha+1)}\Omega(\eta), \qquad \eta = y(-t)^{\alpha}; \tag{A7}$$

these satisfy

$$\Omega_\eta - \alpha\eta\Omega_{\eta\eta} = \Omega_\eta^2 - \Omega\Omega_{\eta\eta} \tag{A8}$$

so that we require $\Omega_\eta = 0$, $\Omega_\eta = 1$ or

$$\Omega_\eta^{\alpha}(1 - \Omega_\eta)^{1-\alpha} = \lambda_0(\alpha\eta - \Omega) \tag{A9}$$

for some constant of integration λ_0. Writing $\Omega = \alpha\eta - \Phi$ in (A9) yields an autonomous equation whose phase plane is readily analysed; moreover,

$$\int_0^{\Omega_\eta} P^{\alpha-1}(1 - P)^{-\alpha}\,\mathrm{d}P = \lambda_0(\eta + \eta_0) \tag{A10}$$

for some constant η_0. Imposing the conditions

$$\text{at } \eta = 0 \qquad \Omega = \Omega_\eta = 0, \tag{A11}$$

so that $\eta_0 = 0$, we have

$$\Omega \sim \frac{\alpha}{\alpha+1}(\lambda_0\alpha)^{1/\alpha}\eta^{(\alpha+1)/\alpha} \qquad \text{as } \eta \to 0^+,$$

and we thus need $\alpha > 0$, $\lambda_0 > 0$. For our purposes the cases

$$\alpha = 1 \qquad \Omega = -\frac{1}{\lambda_0} + \eta + \frac{1}{\lambda_0}\mathrm{e}^{-\lambda_0\eta}, \tag{A12}$$

$$\alpha = \frac{1}{2} \qquad \Omega = \frac{1}{2}\eta - \frac{1}{2\lambda_0}\sin(\lambda_0\eta), \tag{A13}$$

are those of most significance (for reasons which will subsequently become clear). We first consider the condition

$$\text{as } \eta \to +\infty \qquad \Omega_\eta \to 1, \tag{A14}$$

relevant to Section 6.4. This constraint is automatically satisfied for (A9), (A12) when $\alpha \geq 1$, with

$$\Omega_\eta \sim 1 - (\lambda_0(\alpha-1))^{1/\alpha}\eta^{-1/(\alpha-1)} \qquad \text{as } \eta \to +\infty \text{ for } \alpha > 1;$$

the approach to (A14) is therefore most rapid for (A12) and it was shown in Section 6.4 how a 'logarithmically perturbed' version of the $\alpha = 1$ similarity solution is selected by appropriate matching of the exponentially decaying term (in a manner analogous to the way in which a logarithmically perturbed form of the fastest-decaying travelling wave is selected by Fisher's equation; see [34], for example). Equation (A8) also possesses non-analytic solutions which satisfy (A11) and (A14) when $0 < \alpha < 1$; these satisfy (A9) for $\eta < \eta_c$, where $\Omega(\eta_c) = \alpha\eta_c$, $\Omega_\eta(\eta_c) = 1$, and $\Omega = \alpha\eta_c + \eta - \eta_c$ for $\eta > \eta_c$, with

$$\Omega \sim \alpha\eta_c + (\eta - \eta_c) + \frac{1-\alpha}{2-\alpha}(\lambda_0(1-\alpha))^{1/(1-\alpha)}(\eta_c - \eta)^{(2-\alpha)/(1-\alpha)} \qquad \text{as } \eta \to \eta_c^-. \tag{A15}$$

However, for such a solution to be tenable in the current context, it must be realisable as the $\delta \to 0^+$ limit of a solution to the viscous equation

$$\mathcal{F}_{yt} = \delta\mathcal{F}_{yyy} + \mathcal{F}_y^2 - \mathcal{F}\mathcal{F}_{yy}, \tag{A16}$$

with $t \to 0^-$ (where we here use δ to denote the size of the (small) viscous term). Introducing

$$y = s(t) + \delta^{1/2}z, \qquad \mathcal{F} = \dot{s}(t) + \delta^{1/2}\frac{z}{(-t)} + \delta^{(2-\alpha)/2(1-\alpha)}F \tag{A17}$$

to describe the viscous interior layer, where $s(t) \sim \eta_c(-t)^{-\alpha}$, yields to leading order in δ that

$$F_{0zt} = F_{0zzz} + \frac{z}{(-t)}F_{0z} - \frac{z}{(-t)}F_{0zz}. \tag{A18}$$

It is easily seen that the only solutions to (A18) of the form

$$F_0 = (-t)^q\Phi(\zeta), \qquad \zeta = z/(-t)^{1/2} \tag{A19}$$

which do not blow up exponentially in at least one of the limits $\zeta \to \pm\infty$ are polynomials of the form

$$\Phi(\zeta) = k_N \sum_{n=0}^{[N/2]} \gamma_n \zeta^{N-2n}, \qquad q = \tfrac{3}{2}(N-2), \tag{A20}$$

where N is a non-negative integer, k_N is arbitrary, $\gamma_0 = 1$ and the other γ_n can be determined from (A18). It is also readily confirmed that (A19–A20) provide the only relevant solutions to (A18) in the limit $t \to 0^-$; since it is not possible to match any of these both with (A15) as $z \to -\infty$ and with $\Omega = \alpha\eta_c + \eta - \eta_c$ as $z \to +\infty$, the case $\alpha < 1$ can thus be ruled out, further clarifying the reasons why (A12) is the solution that arises when describing the relevant intermediate asymptotic behaviour.

In Section 7.1 a condition corresponding to

$$\text{as } \eta \to +\infty \qquad \Omega \to \Omega_\infty \tag{A21}$$

applies (in addition to (A11)), where the constant Ω_∞ needs to be determined as part of the solution. As already indicated, this condition cannot be satisfied for $\alpha \geq 1$ when (A11) holds; for particular $\alpha < 1$, however, we can construct a suitable solution in two parts, comprising a solution to (A8) with $\Omega_\eta \not\equiv 0, 1$ for $\eta < 2\eta_c$, with $\Omega(2\eta_c) = 2\alpha\eta_c$, $\Omega_\eta(2\eta_c) = 0$, and $\Omega = 2\alpha\eta_c$ for $\eta > 2\eta_c$ (the quantity η_c is given by (A22) below, with $\Omega_\infty = 2\alpha\eta_c$). However, before discussing the acceptability of such a non-analyticity at $\eta = 2\eta_c$, we need to consider the behaviour close to $\eta = \eta_c$, since $\Omega_\eta(\eta_c) = 1$, implying that the analysis of (A18) described above becomes relevant; using (A10) we have

$$\lambda_0\eta_c = \int_0^1 P^{\alpha-1}(1-P)^{-\alpha}\,\mathrm{d}P. \tag{A22}$$

The inner solutions (A20) are now viable, requiring to match with (A15) as $z \to -\infty$ that

$$\alpha = \frac{N-2}{N-1}, \qquad k_N = \frac{1}{N}\left(\frac{\lambda_0}{N-2}\right)^{-(N-2)}. \tag{A23}$$

However, to continue the solution into $\eta > \eta_c$ it is necessary that N be an odd integer; then for $\eta_c < \eta < 2\eta_c$ we can replace λ_0 in (A9) by $-\lambda_0$ and take

$$\Omega(\eta) = 2\alpha\eta_c - \Omega(2\eta_c - \eta) \tag{A24}$$

(such a change of signs in (A9) is already implicit in (A13)). We deduce, therefore, that a similarity solution of the form (A7) satisfying (A10) and (A21) is realisable only when α is given by (A23), wherein $N > 1$ is an odd integer. Moreover, the preceding analysis of (A18) indicates that the generic case is $N = 3$, $\alpha = \frac{1}{2}$, explaining its occurrence in the analysis of Section 7.1. For $\alpha = \frac{1}{2}$, we have from (A13) that $\eta_c = \pi/\lambda_0$.

Finally, we need to explain the reasons for the acceptability of the non-analyticity in the solution at $\eta = 2\eta_c$. (We note that more than one oscillation in, say, (A13) could in principle occur before the solution switches to $\Omega = \Omega_\infty$, but the case $\eta_c = \pi/\lambda_0$ is expected to be generic, rather than $\eta_c = M\pi/\lambda_0$ for some integer $M > 1$.) As $\eta \to 2\eta_c^-$ we have from (A9) that

$$\Omega \sim 2\alpha\eta_c + \frac{\alpha}{\alpha+1}(\alpha\lambda_0)^{1/\alpha}(2\eta_c - \eta)^{(\alpha+1)/\alpha}. \tag{A25}$$

The inner scalings for (A16) thus now read

$$y = s(t) + \delta^{1/2} z, \qquad \mathcal{F} = \dot{s}(t) + \delta^{(\alpha+1)/2\alpha} F \tag{A26}$$

with, in this case, $s(t) \sim 2\eta_c(-t)^{-\alpha}$, leading in place of (A18) to

$$F_{0zt} = F_{0zzz}, \tag{A27}$$

from which it follows that

$$F_0(z,t) \sim \Phi_0(z) \qquad \text{as } t \to 0^-,$$

where viscous effects play no role and $\Phi_0(z)$ is arbitrary (being determined by the evolution over earlier times) except that it satisfies

$$\Phi_0 \sim \frac{\alpha}{\alpha+1}(\alpha\lambda_0)^{1/\alpha}(-z)^{(\alpha+1)/\alpha} \qquad \text{as } z \to -\infty,$$
$$\Phi_0 \to 0 \qquad \text{as } z \to +\infty.$$

Hence the interior layer (A26–A27) places no constraints on the value of α, the only active role played by viscous effects in the discussion of this appendix being confined to the interior layer described by (A17–A18), which plays a crucial role in selecting the value $\alpha = \frac{1}{2}$. Although viscosity plays no explicit role in Section 7.1.2, the inner analysis about $\eta = \eta_c$ described above implies the requirement on the inviscid solution that it be analytic where $\mathcal{F}_y$ is maximal; such a constraint is implicit in the derivation of (132). We note that $\omega = x\mathcal{F}_{yy} = 0$ at both $\eta = \eta_c$ and $\eta = 2\eta_c$ and, in view of (A4), both are therefore characteristics of (A1).

Appendix B. Symmetries of the viscous Riabouchinsky–Proudman–Johnson equation

This appendix is concerned with the symmetries of (1) and briefly indicates some of their implications. This partial differential equation is invariant under translations of both y and t,

$$y^* = y + y_0, \quad t^* = t + t_0, \quad \mathcal{F}^* = \mathcal{F}, \tag{B1}$$

and has a scaling invariant

$$y^* = \sigma y, \quad t^* = \sigma^2 t, \quad \mathcal{F}^* = \mathcal{F}/\sigma \tag{B2}$$

(with the inviscid case $\epsilon = 0$ having another) which implies the existence of the similarity reductions

$$\mathcal{F}(y,t) = (\pm t)^{1/2}\Omega(\eta), \qquad \eta = y/(\pm t)^{1/2} \tag{B3}$$

which fail, however, to feature in our asymptotic analysis (though only just – see (101)). More interesting is the infinite-dimensional Galilean symmetry

$$y^* = y - s(t), \qquad t^* = t, \qquad \mathcal{F}^*(y^*,t^*) = \mathcal{F}(y,t) - \dot{s}(t) \tag{B4}$$

where $s(t)$ is arbitrary. This symmetry has an implicit role in the analysis of a number of the interior layers appearing above and it implies the obvious result that $\mathcal{F} = a(t) + b(t)y$ satisfies (1) for any $a(t)$ and $b(t)$. Moreover, it leads, together with (B1), to the similarity reduction

$$\mathcal{F}(y,t) = \dot{s}(t) + \Omega(\eta), \qquad \eta = y - s(t), \tag{B5}$$

which has steady states and travelling waves as special cases (with the particular implication that steady-state results carry over directly to the more general class of solutions (B5)), and, together with (B2), to

$$\mathcal{F}(y,t) = \dot{s} + (\pm t)^{1/2}\Omega(\eta), \qquad \eta = (y - s(t))/(\pm t)^{1/2}. \tag{B6}$$

Another noteworthy feature of (1) is its quadratically nonlinear form, which we have already exploited to obtain low-dimensional reductions, giving solutions which cannot be obtained by classical similarity methods. The relevant invariant subspaces are preserved under (B1), (B2) and (B3), so (prior to the imposition of boundary conditions) the resulting ordinary differential equations inherit each of these symmetries; it is worth noting that the invariant subspaces include useful special cases of (68) of the form

$$\mathcal{F} = a(t) + b(t)y + c(t)\mathrm{e}^{-\lambda(t)y}, \qquad \mathcal{F} = a(t) + c(t)\mathrm{e}^{-\kappa y}.$$

References

1. D. Riabouchinsky, Quelques considérations sur les mouvements plans rotationnels d'un liquide. *C. R. Hebd. Acad. Sci.* 179 (1924) 1133–1136.
2. I. Proudman and K. Johnson, Boundary-layer growth near a rear stagnation point. *J. Fluid Mech.* 12 (1962) 161–168.
3. K. Hiemenz, Die Grenzschicht an einem in den gleichförmigen Flüssigkeitsstrom eingetauchten geraden Kreiszylinder. *Dinglers Polytech. J.* 326 (1911) 321–324, 344–348, 357–362, 372–376, 391–393, 407–410.
4. A. S. Berman, Laminar flow in channels with porous walls. *J. Appl. Phys.* 24 (1953) 1232–1235.
5. R. M. Terrill, On some exponentially small terms arising in flow through a porous pipe. *Quart. J. Mech. Appl. Math.* 26 (1973) 347–354.
6. R. E. Grundy and H. R. Allen, The asymptotic solution of a family of boundary value problems involving exponentially small terms. *IMA J. Appl. Math.* 53 (1994) 151–168.
7. S. M. Cox and A. C. King, On the asymptotic solution of a high order non-linear ordinary differential equation. *Proc. R. Soc. London* A 453 (1997) 711–728.
8. R. M. Terrill, Laminar flow in a uniformly porous channel. *Aeronaut. Quart.* 15 (1964) 299–310.
9. M. B. Zaturska, P. G. Drazin and W. H. H. Banks, On the flow of a viscous fluid driven along a channel by suction at porous walls. *Fluid Dyn. Res.* 4 (1988) 151–178.
10. I. Proudman, An example of steady laminar flow at large Reynolds number. *J. Fluid Mech.* 9 (1960) 593–602.
11. R. M. Terrill and G. M. Shrestha, Laminar flow through parallel and uniformly porous walls of different permeability. *ZAMP* 16 (1965) 470–482.
12. R. M. Terrill and G. M. Shrestha, Laminar flow through a channel with uniformly porous walls of different permeability. *Appl. Sci. Res.* 15 (1966) 440–468.
13. R. M. Terrill, Flow through a porous annulus. *Appl. Sci. Res.* 17 (1967) 204–222.
14. G. M. Shrestha and R. M. Terrill, Laminar flow with large injection through parallel and uniformly porous walls of different permeability. *Quart. J. Mech. Appl. Math.* 21 (1968) 413–432.
15. S. M. Cox, Two-dimensional flow of a viscous fluid in a channel with porous walls. *J. Fluid Mech.* 227 (1991) 1–33.
16. S. M. Cox, Analysis of steady flow in a channel with one porous wall, or with accelerating walls. *SIAM J. Appl. Math.* 51 (1991) 429–438.
17. R. E. Grundy and R. McLaughlin, Global blow-up of separable solutions of the vorticity equation. *IMA J. Appl. Math.* 59 (1997) 287–307.
18. F. M. Skalak and C.-Y. Wang, On the nonunique solutions of laminar flow through a porous tube or channel. *SIAM J. Appl. Math.* 34 (1978) 535–544.
19. R. M. Terrill, Laminar boundary-layer flow near separation with and without suction. *Phil. Trans. R. Soc. London A* 253 (1960) 55–100.
20. G. N. Mercer and A. J. Roberts, A centre manifold description of contaminant dispersion in channels with varying flow properties. *SIAM J. Appl. Math.* 50 (1990) 1547–1565.

21. C. Domb and M. F. Sykes, On the susceptibility of a ferromagnetic above the Curie point. *Proc. R. Soc. London* A 240 (1957) 214–228.
22. G. K. Batchelor, *An Introduction to Fluid Dynamics*. Cambridge: Cambridge University Press (1967) 615pp.
23. P. G. Drazin and Y. Tourigny, Numerical study of bifurcations by analytic continuation of a function defined by a power series. *SIAM J. Appl. Math.* 56 (1996) 1–18.
24. D. Gottlieb and S. A. Orszag, *Numerical Analysis of Spectral Methods: Theory and Applications*. Philadelphia: SIAM CBMS-MSF Regional Conference Series in Applied Mathematics (1977) 170pp.
25. V. A. Galaktionov and S. A. Posashkov, New exact solutions of parabolic equations with quadratic nonlinearities. *USSR Comput. Maths. Math. Phys.* 21 (1989) 112–119.
26. J. R. King, Mathematical analysis of a model for substitutional diffusion. *Proc. R. Soc. London* A 430 (1990) 377–404.
27. G. I. Barenblatt, *Scaling, Self-Similarity and Intermediate Asymptotics*. Cambridge University Press (1996) 386pp.
28. S. J. Chapman, J. R. King and K. L. Adams, Exponential asymptotics and Stokes lines in nonlinear ordinary differential equations. *Proc. R. Soc. London* A 454 (1998) 2733–2755.
29. M. Van Dyke, *Perturbation Methods in Fluid Mechanics*. Stanford: Parabolic Press (1975) 271pp.
30. J. R. King, 'Instantaneous source' solutions to a singular nonlinear diffusion equation. *J. Eng. Math.* 27 (1993) 31–72.
31. M. A. Goldshtik and N. I. Javorsky, On the flow between a porous rotating disk and a plane. *J. Fluid Mech.* 207 (1989) 1–28.
32. C. L. Taylor, W. H. H. Banks, M. B. Zaturska and P. G. Drazin, Three-dimensional flow in a porous channel. *Quart. J. Mech. Appl. Math.* 44 (1991) 105–133.
33. V. A. Galaktionov and J. L. Vazquez, Blow-up of solutions with free boundaries for the Navier–Stokes equations. Department of Mathematics Preprint 9824, University of Bath, 1998.
34. H. P. McKean, Application of Brownian motion to the equation of Kolmogorov–Petrovskii–Piskunov. *Commun. Pure Appl. Math.* 28 (1975) 323–331. Corrigendum *Commun. Pure Appl. Math.* 29 (1976) 553–554.